

ČESKÉ VYSOKÉ UČENÍ TECHNICKÉ V PRAZE
FAKULTA STROJNÍ
ÚSTAV MECHANIKY, BIOMECHANIKY A MECHATRONIKY



BAKALÁŘSKÁ PRÁCE

NUMERICKÁ SIMULACE ŘEZÁNÍ DŘEVA ŘETĚZOVOU PILOU
NUMERICAL SIMULATION OF WOOD CUTTING BY A CHAINSAW

AUTOR:	MICHAL KOCOUREK
STUDIJNÍ PROGRAM:	TZSI
VEDOUCÍ PRÁCE:	Ing. MARTIN NESLÁDEK Ph.D.

PRAHA 2020

I. OSOBNÍ A STUDIJNÍ ÚDAJE

Příjmení: **Kocourek** Jméno: **Michal** Osobní číslo: **474840**
Fakulta/ústav: **Fakulta strojní**
Zadávající katedra/ústav: **Ústav mechaniky, biomechaniky a mechatroniky**
Studijní program: **Teoretický základ strojního inženýrství**
Studijní obor: **bez oboru**

II. ÚDAJE K BAKALÁŘSKÉ PRÁCI

Název bakalářské práce:

Numerická simulace řezání dřeva řetězovou pilou

Název bakalářské práce anglicky:

Numerical simulation of wood cutting by a chainsaw

Pokyny pro vypracování:

1. Proveďte rešerši na téma materiálových mechanických vlastností bukového dřeva. Seznamte se s možností modelování porušování materiálu v programu LS-Dyna. Poznátky vhodně zpracujte v rešeršní kapitole bakalářské práce.
2. V programu LS-Dyna vytvořte simulační model experimentálního měření silových poměrů při řezání zubem řetězové pily s uvažováním vhodného modelu porušování materiálu v místě řezu.
3. Verifikujte numerický model pomocí experimentálně měřených dat a případně proveďte korekci parametrů modelu pro získání lepší shody.
4. Výsledky práce vhodně zpracujte a shrňte v závěrečné zprávě.

Seznam doporučené literatury:

- [1] manuály LS-Dyna
- [2] Holan, J., Merenda, L.: Selected mechanical properties of modified beech wood. Acta univ. agric. et silvic. Mendel. Brun., LVI, No. 1, pp. 245–250 (2008).
- [3] Green, D.W., Winandy, J.E., Kretschmann, D.E.: Mechanical Properties of Wood. Wood handbook: wood as an engineering material. Madison, WI : USDA Forest Service, Forest Products Laboratory. General technical report FPL; GTR-113: pp. 4.1–4.45 (1999).

Jméno a pracoviště vedoucí(ho) bakalářské práce:


Ing. Martin Nesládek, Ph.D., ústav mechaniky, biomechaniky a mechatroniky FS

Jméno a pracoviště druhé(ho) vedoucí(ho) nebo konzultanta(ky) bakalářské práce:

Datum zadání bakalářské práce: **15.04.2020**

Termín odevzdání bakalářské práce: **07.08.2020**

Platnost zadání bakalářské práce:



Ing. Martin Nesládek, Ph.D.
podpis vedoucí(ho) práce



doc. Ing. Miroslav Španiel, CSc.
podpis vedoucí(ho) ústavu/katedry



prof. Ing. Michael Valášek, DrSc.
podpis děkana(ky)

III. PŘEVZETÍ ZADÁNÍ

Student bere na vědomí, že je povinen vypracovat bakalářskou práci samostatně, bez cizí pomoci, s výjimkou poskytnutých konzultací. Seznam použité literatury, jiných pramenů a jmen konzultantů je třeba uvést v bakalářské práci.

14.7.2020

Datum převzetí zadání



Podpis studenta

ANOTAČNÍ LIST

Jméno autora:	Michal Kocourek	
Název BP:	Numerická simulace řezání dřeva řetězovou pilou	
Anglický název:	Numerical simulation of wood cutting by a chainsaw	
Rok:	2020	
Zadávací ústav:	Ústav mechaniky, biomechaniky a mechatroniky	
Vedoucí BP:	Ing. Martin Nesládek, Ph.D.	
Bibliografické údaje:	Počet stran	82
	Počet obrázků	42
	Počet grafů	15
	Počet tabulek	7
	Počet příloh	1
Klíčová slova:	Metoda konečných prvků, dřevo, řezné síly, motorová pila	
Keywords:	Finite Element Method, Wood, Cutting Forces, Chainsaw	
Anotace:	Tato bakalářská práce se zabývá kalibrací materiálového modelu bukového dřeva s použitím realistických materiálových vlastností v programu LS Dyna pro simulace metodou konečných prvků. Vlastosti byly nalezeny v literatuře a výsledný model ukazuje dobrou shodu s experimentem jak po stránce řezných sil, tak z hlediska tvorby třísky.	
Annotation:	This bachelor thesis deals with calibration of a material model of beech wood using realistic material properties in the LS Dyna software for finite element method simulations. The properties were extracted from the literature and the final model shows good match with the experiment both in the cutting forces and the chip formation.	

PROHLÁŠENÍ

Prohlašuji, že jsem bakalářskou práci s názvem: „Numerické simulace procesu řezání dřeva“ vypracoval samostatně pod vedením Ing. Martina Nesládky, Ph.D. a s použitím literatury uvedené na konci mé bakalářské práce v seznamu použité literatury.

DECLARATION

I declare that this thesis, by the name “Numerical simulations of the wood cutting process” was created solely by me, with the help of my thesis supervisor Ing. Martin Nesládek, Ph.D. and the literature provided at the end of this thesis in the list of references.

Prague

Michal Kocourek

PODĚKOVÁNÍ

Rád bych zde poděkoval vedoucímu mé bakalářské práce Ing. Martinu Nesládkovi, Ph.D. za jeho vedení a čas, který mi věnoval. Dále bych rád poděkoval svým kolegům v práci, zejména Ing. Lukáši Horáčkovi, za odborné rady a pomoc.

ACKNOWLEDGEMENT

I would like to thank my thesis supervisor Ing Martin Nesládek, Ph.D. for his guidance and the time, he spent helping me with my thesis. I would also like to thank my colleagues, primarily Ing. Lukáš Horáček for the expert advice and help.

Table of Contents

1	Introduction.....	10
2	Literature Review.....	12
2.1	Material properties of European beech wood.....	12
2.1.1	Density	13
2.1.2	Normal Elastic Moduli.....	14
2.1.3	Shear Elastic Moduli	14
2.1.4	Poisson's ratios.....	15
2.1.5	Tensile Strength	16
2.1.6	Compressive Strength	17
2.1.7	Shear strength.....	17
2.2	Methods for Experimental Determination of Mechanical Properties of Wood	18
2.2.1	Digital Image Correlation	18
2.2.2	Tensile Tests.....	18
2.2.3	Compression Tests	19
2.2.4	Torsion Test	20
2.2.5	A Special Shear Testing Method.....	21
2.2.6	Ultrasonic Wave Utilization.....	22
2.3	Wood Failure Simulation in LS-DYNA.....	23
2.3.1	Material Model.....	24
2.3.2	Elastic Properties.....	24
2.3.3	Failure Criteria	25
2.4	Basics of the Mathematics Behind the Explicit and Implicit Finite Element Method Computations.....	27
2.4.1	Explicit simulations.....	27
2.4.2	Implicit simulations.....	28
3	Experiment.....	30
3.1	Setup.....	30
3.2	Measurements.....	31
3.3	Evaluation.....	32
3.4	Results	33

4	Investigation of the Sensitivity of the Numerical Simulations on Individual Parameters.....	38
4.1	Chip Formation.....	38
4.1.1	Version 1.00 – First Attempt.....	38
4.1.2	Version 1.01 – Timestep Decreased.....	45
4.1.3	Version 1.02 – Material Data from the Literature.....	45
4.1.4	Finding the Problem.....	46
4.1.5	Element formulation.....	48
4.1.6	Poisson’s Ratio.....	48
4.1.7	Parallel Normal Modulus	49
4.1.8	Version 1.11 – Perpendicular Shear Modulus.....	50
4.1.9	Version 1.12 – IFAIL on.....	51
4.1.10	Version 1.13 – Timestep Further Decreased.....	52
4.2	Contact Forces	52
4.2.1	Version 2.00 – The First Model	55
4.2.2	Version 2.01 – Friction Increased	56
4.2.3	Version 2.02 – Thicker Wood.....	58
4.2.4	Timestep variation.....	58
4.2.5	Mesh size variation	58
4.2.6	Contact definition.....	59
4.2.7	Contact scaling	60
4.2.8	Elastic Moduli	61
4.2.9	Failure Criteria	61
4.2.10	Poisson’s Ratio.....	63
4.2.11	Softening Parameters	63
4.2.12	Hardening Parameters	63
5	Final Version.....	65
5.1	Contact Forces	65
5.1.1	Mesh.....	66
5.1.2	Simulation Settings	66
5.1.3	Evaluation	67
5.1.4	Results.....	67

5.2	Chip Formation.....	69
5.2.1	Results.....	69
6	Conclusion.....	71
	References.....	72
	List of Figures.....	75
	List of Tables.....	77
	Appendix I – Tables of the mechanical properties of the beech wood.....	78

1 Introduction

This thesis was created in collaboration with the companies AKKA Czech Republic s.r.o. (AKKA) and Andreas STIHL AG & Co. KG (STIHL).

In AKKA, there was an attempt to develop a large and complicated finite elements method (FEM) simulation of chainsaw cutting. Although the simulation was a huge success, unphysical mechanical properties of wood (i.e. differing by orders of magnitude) had to be used, in order to match the cutting forces with reality. This thesis aims to investigate the influence of the input parameters on the simulated cutting forces and calibrate an available material model of beech wood using realistic mechanical properties that could later be used in this simulation to bring it another step further.

A specialized experiment for the cutting forces measurement during wood cutting was set. The experiment layout is shown in Fig. 1. Experimental data used for the calibration of the numerical models were provided by STIHL. The cutting forces and the chip formation are considered during the calibration.

The explicit method is used for the computation because of its simplicity and no necessity for solving the dynamic equilibrium iteratively. Basic differences between the explicit and the implicit method are discussed further. The software LS-DYNA was used to carry out the simulations. LS-DYNA is a multi-purpose solver used for analysing the large deformation static and dynamic response of structures, mainly by the explicit method.

The material subjected to testing was European beech wood. Material data required for the FEM simulation were not provided and thus are extracted from the literature. It is important to state, that wood is a very variable material (i.e. the material properties vary piece by piece). Therefore, a range of possible mechanical properties is searched, rather than exact values.

The principal aim of this thesis is creating a working LS-Dyna simulation matching the wood cutting experiment in terms of cutting forces and wooden chip shape as close as possible.

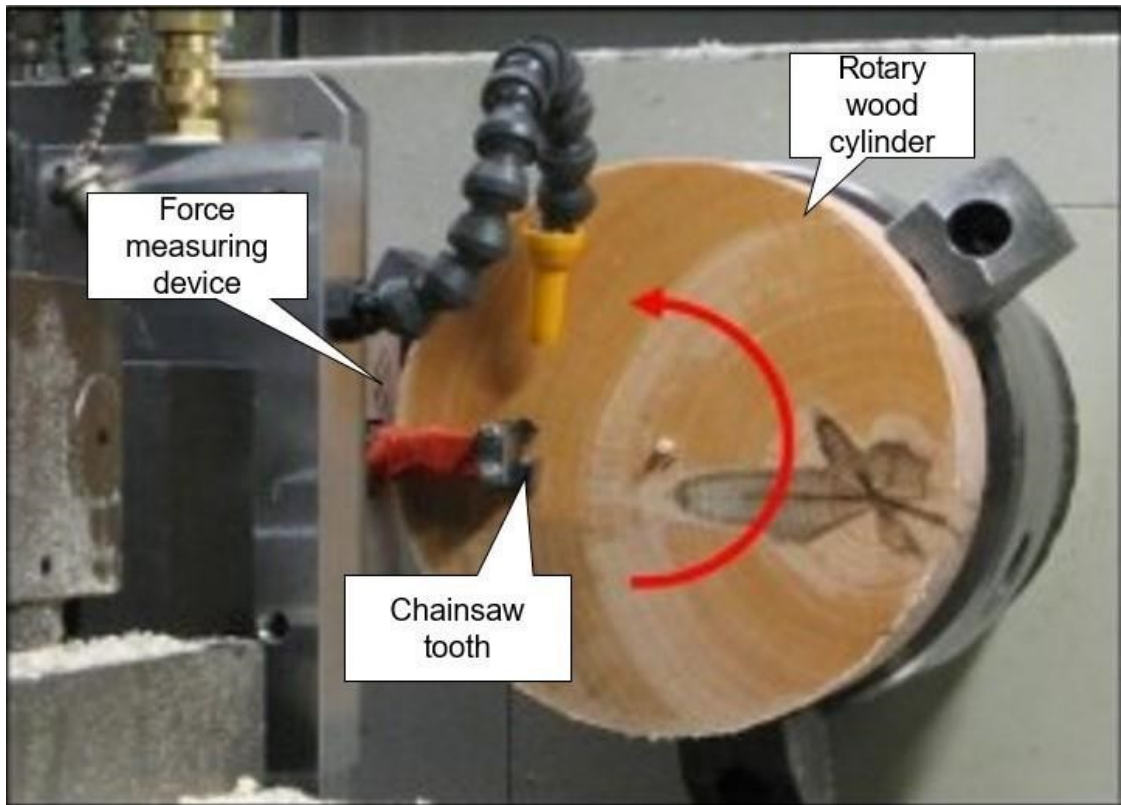


Fig. 1 - View of the experimental setup used to determine the cutting forces acting on a single chainsaw tooth

2 Literature Review

In this chapter, the mechanical behaviour of wood is discussed along with the testing methods. Also, the mathematics behind the FEM calculations and the failure criteria model are briefly introduced.

2.1 Material properties of European beech wood

Wood is composed of inhomogeneous organic tissue, which makes it difficult to describe its mechanical properties generally. The behaviour of wood changes significantly with different moisture content (MC) and quality. It is a hierarchical material, having a different structure on several levels. [1]

It is common to idealize wood as having different mechanical properties in three mutually perpendicular directions – longitudinal to the grain, and tangential, and radial to the annual rings, which are shown in Fig. 2. This indicates that wood is an orthotropic material. However, some sources suggest that wood does not exhibit elastic orthotropic symmetry [2]. Wood divides into hardwoods and softwoods. Hardwoods are usually denser than softwoods making them a better fit for forestry equipment testing.

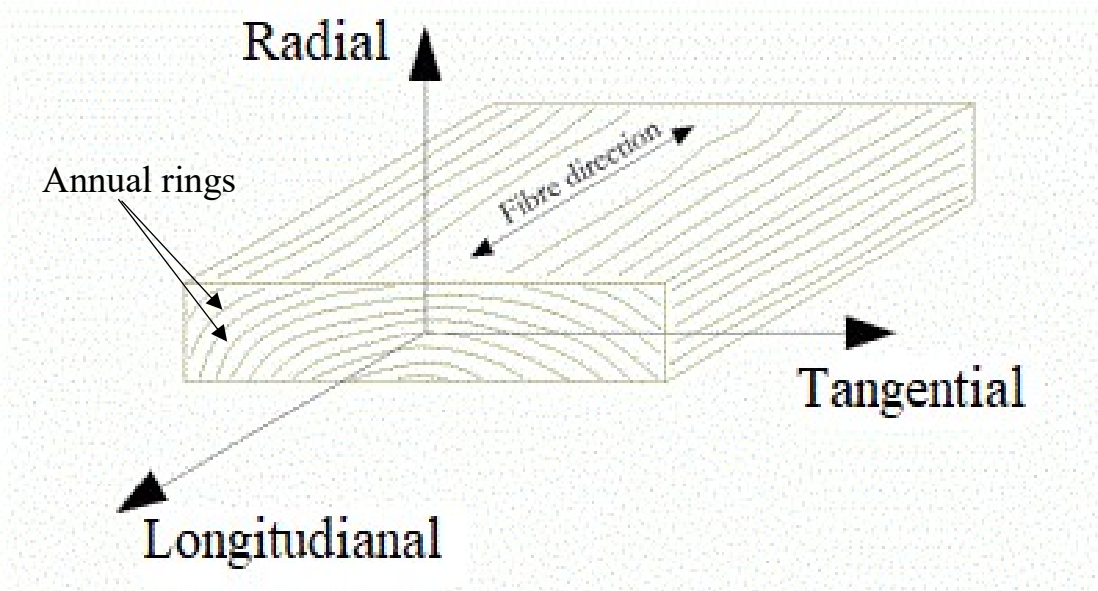


Fig. 2 - Material axes of wood [3]

Wood from the European beech (*Fagus Sylvatica L.*), which ranks among hardwoods, has been used for the experiment of wood cutting. To calibrate the material model with realistic values, moisture dependent mechanical properties of beech wood have been extracted from the literature, put together and analysed. Moisture dependency could help with finding optimal values since the MC of the wood specimen is standardized for the wood cutting experiment. Individual properties are discussed in chapters 2.1.1 to 2.1.6. The data are summarised in Appendix I with references to the literature. Coefficient of determination (CoD) has been used for each mechanical property to distinguish, whether it exhibits moisture dependency.

2.1.1 Density

Contrary to the expectations, the density did not show any apparent moisture dependency as can be seen in Fig. 3, with the CoD for linear regression being less than 0.16. This may be caused by the wood expanding simultaneously with increasing MC. The density was first calculated as: 653 kg/m^3 with a standard deviation of 76 kg/m^3 . Using the empirical rule, it can be said that the value 312 kg/m^3 is incorrect with a certainty exceeding 99.7 % and is therefore considered a typing error and neglected. The CoD would then be less than 0.06.

The recalculated value of the density was $667 \pm 33 \text{ kg/m}^3$.

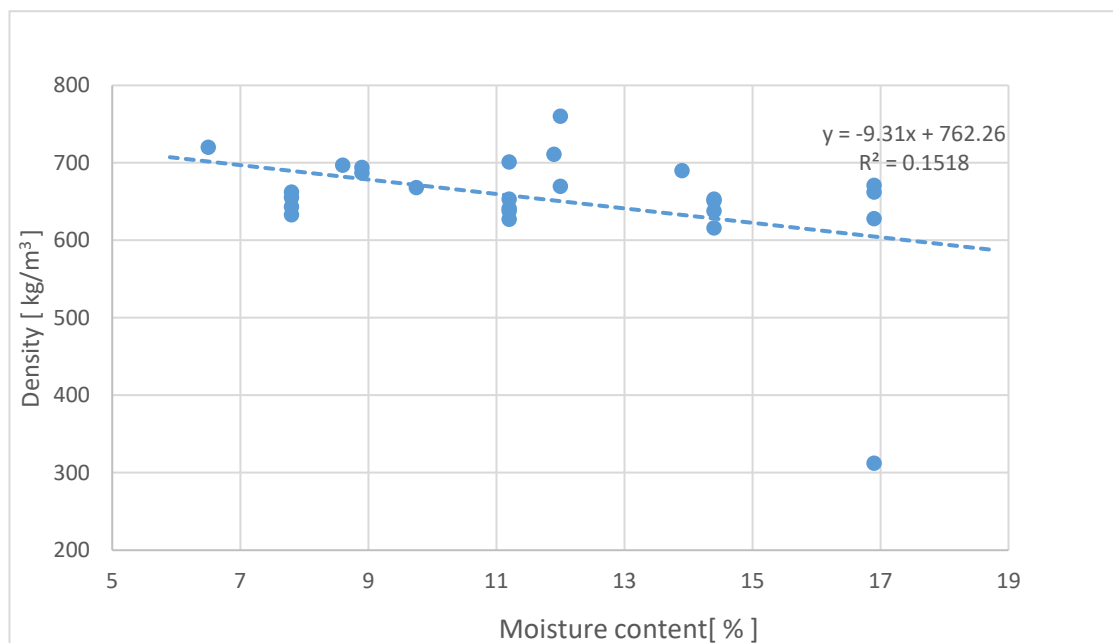


Fig. 3 - Moisture dependent density

2.1.2 Normal Elastic Moduli

The normal elastic moduli show linear decrease with the CoD 0.612, 0.347 and 0.065 for the longitudinal, radial, and tangential directions, respectively.

Linear approximation has been used for all elastic moduli despite the low CoD of the tangential elastic modulus regression, because the other two elastic moduli exhibit considerable moisture dependencies. Fig. 4 shows normal elastic moduli in relation to MC.

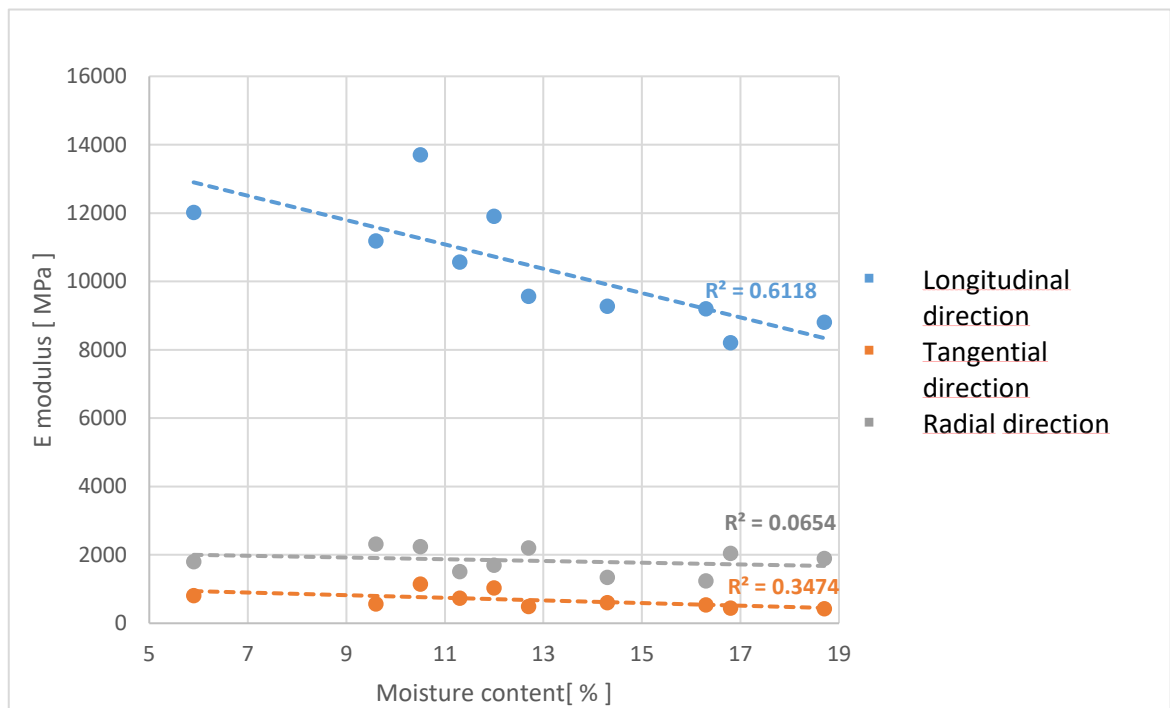


Fig. 4 - Moisture dependent normal elastic moduli

2.1.3 Shear Elastic Moduli

For the shear elastic moduli, using the linear regression no value of CoD exceeded 0.03. Approximation by other functions showed no significant simultaneous increase in CoD unless high degree polynomial functions were used, with the CoD in the LR direction still not exceeding 0.17 when a 6th degree polynomial function approximation is used. No moisture dependency is therefore considered. The moisture dependency of the shear moduli is shown in Fig. 5.

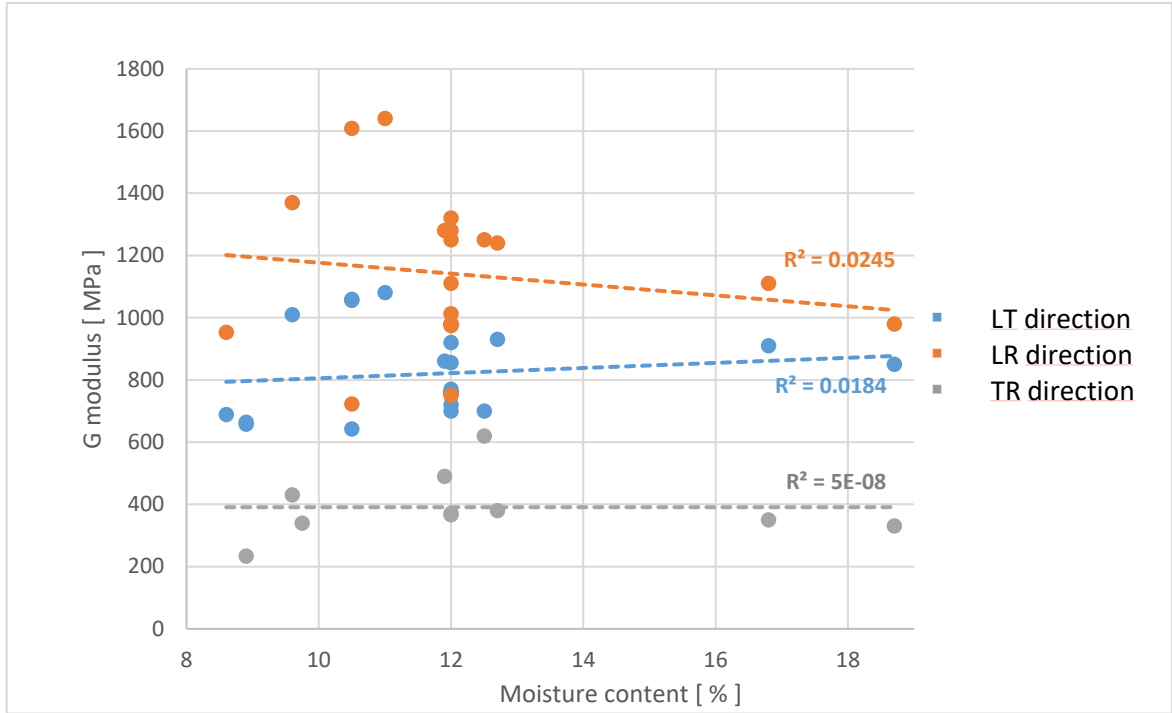


Fig. 5 – Moisture dependent elastic shear moduli

2.1.4 Poisson's ratios

In some directions, the values from different sources differ considerably. Some sources even state Poisson's ratios exceeding 1.

If Poisson's ratio ν_{TL} is defined as the negative ratio between the deformations in the tangential and the longitudinal direction caused by a load in the longitudinal direction:

$$\nu_{TL} = -\frac{\varepsilon_T}{\varepsilon_L} \quad (1)$$

and the relative volume change is in simplified form defined as:

$$\theta = \varepsilon_L + \varepsilon_T + \varepsilon_R = \varepsilon_L - \varepsilon_L \cdot \nu_{TL} - \varepsilon_L \cdot \nu_{RL} \quad (2)$$

then the ν_{TL} value exceeding 1 would suggest that tensile load in the longitudinal direction causes negative volume change for any positive ν_{RL} , which is not reasonably explicable.

It is therefore important to distinguish between the ways of acquiring the values. The values exceeding 1 are not measured directly but calculated assuming perfect orthotropic

symmetry which is therefore considered not to be fulfilled. [2] The moisture dependent Poisson's ratios are shown in Fig. 6.

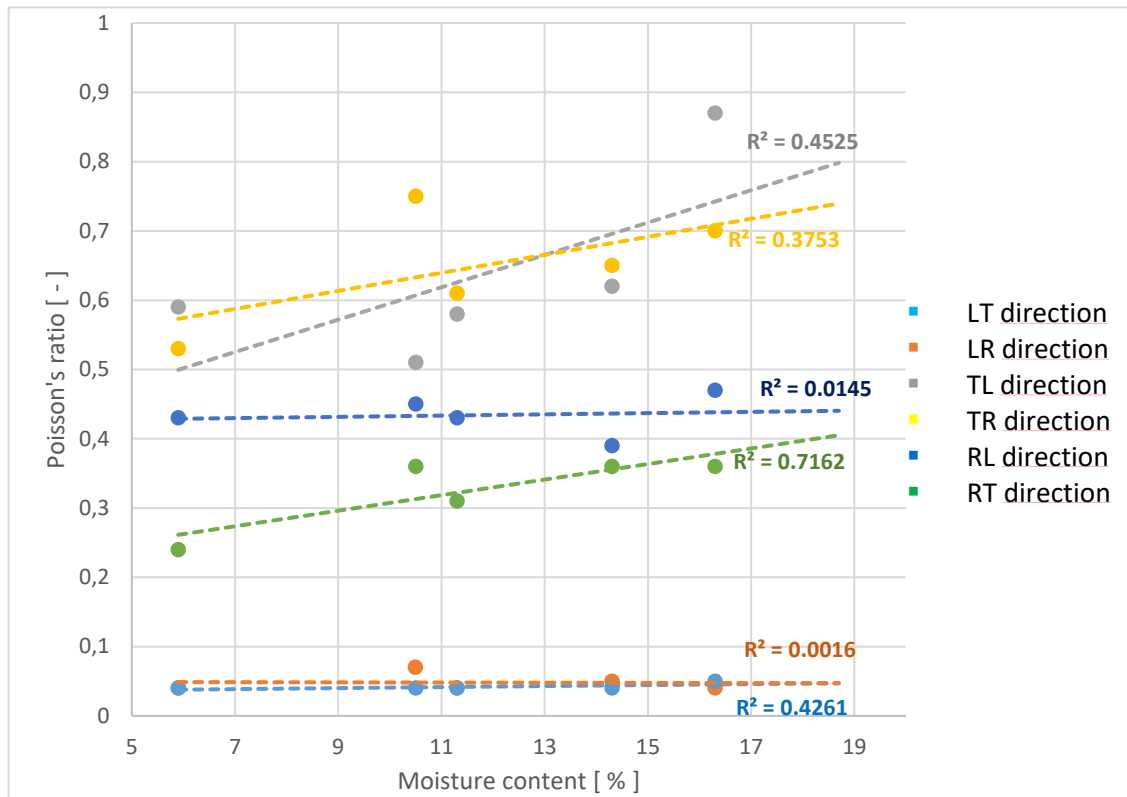


Fig. 6 - Moisture dependent Poisson's ratios (the calculated values are not included)

When the calculated values are not considered, Poisson's ratios ν_{TL} , ν_{TR} , ν_{RT} and ν_{LT} exhibit increasing linear moisture dependency with CoD over 0.35. Surprisingly, for the remaining two Poisson's ratios the CoD values do not exceed 0.04.

2.1.5 Tensile Strength

Few sources state a value of tensile strength. For the data acquired, the CoD for linear regression of the L, T and R directions were 0.482, 0.958 and 0.989 respectively, with strength decrease over increasing MC. It is apparent, that for the longitudinal direction, where data from more than one source were used, the CoD is significantly lower. It is important to say, however, that each value is already a mean value acquired from multiple testing. The CoD decrease can be explained by using different testing methods and measuring equipment. This needs to be considered when choosing the optimal value for the material model. The moisture dependent tensile strengths are shown in Fig. 7.

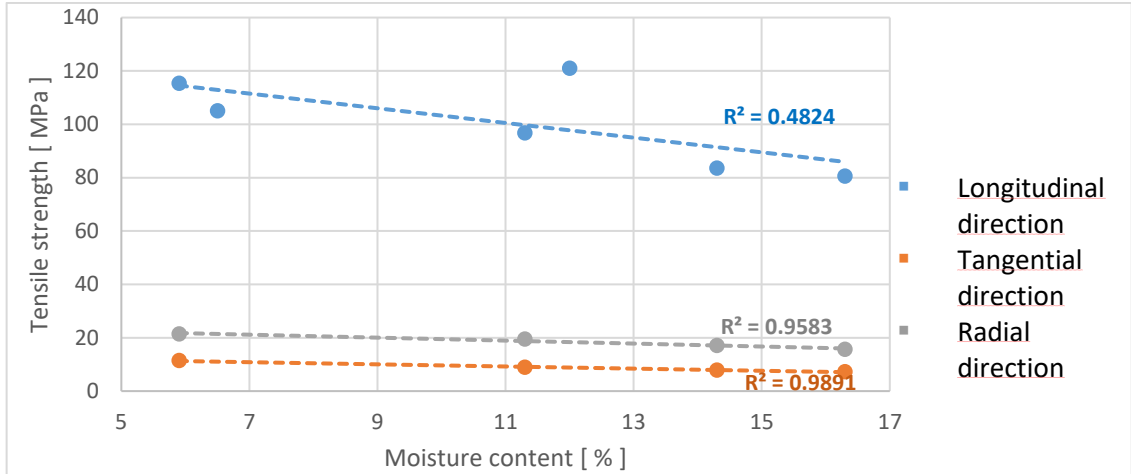


Fig. 7 - Moisture dependent tensile strengths

2.1.6 Compressive Strengths

Data for the compressive strength have been obtained from three sources, one differing significantly from the other two in the perpendicular directions (values 6, 12.9, and 52.3 N · mm⁻² for the tangential direction and 11, 8.5, and 52.4 N · mm⁻² for the radial direction). The data from the two sources were used. It must be born in mind, though, when tuning the material model. The compressive strength has small amount of data and graph of its moisture dependency would not give the reader any new insight.

2.1.7 Shear strengths

The values of shear strength vary considerably even for a single MC value (Fig. 8). The range, in which the optimal shear strength values will be searched will therefore be wide.

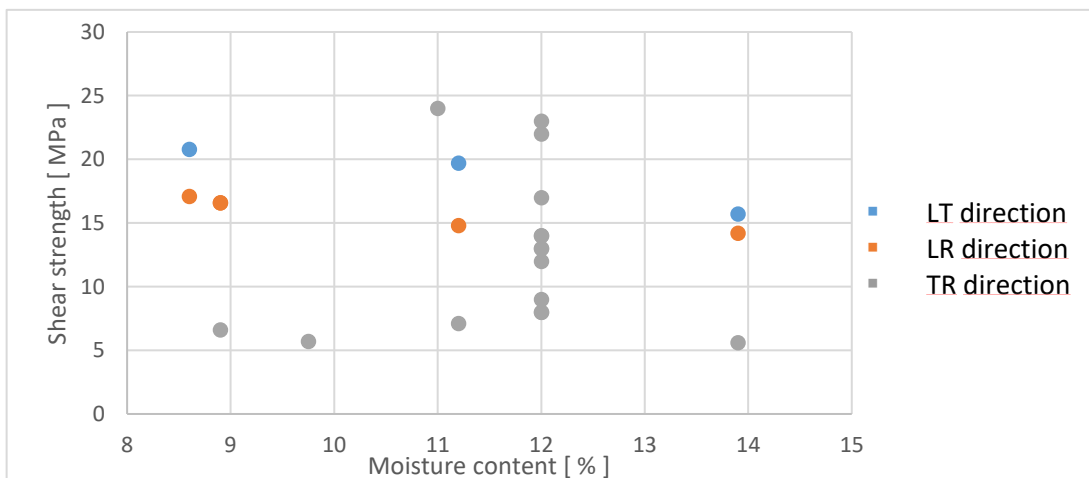


Fig. 8 - Moisture dependent shear strength

2.2 Methods for Experimental Determination of Mechanical Properties of Wood

In this chapter, the methods used in literature for determining the mechanical properties of wood are discussed. Standard testing methods similar to those used for testing steel, as well as new, modern methods are presented.

2.2.1 Digital Image Correlation

Digital image correlation (DIC) is a method of deformation measurement based on optical comparison of the undeformed and deformed object. Random patterns are sprayed on the measured area enabling the computer to distinguish between individual points on the specimen. Comparing the position of individual points before and after the deformation allows us to evaluate the strains (Fig. 9). [4] [5]

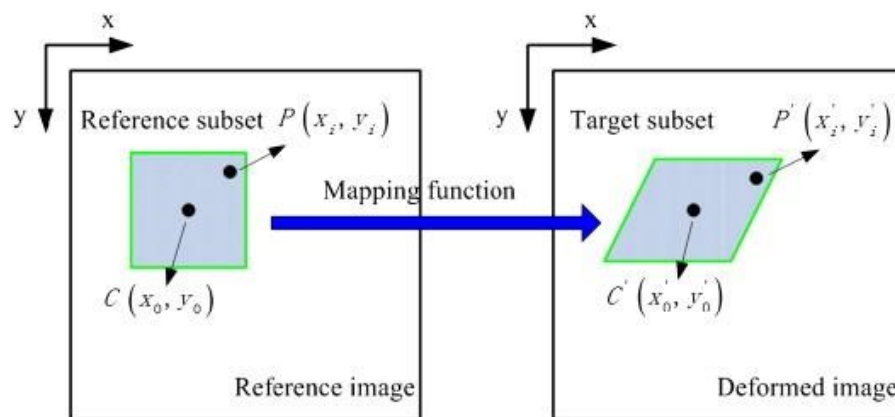


Fig. 9 - The principle of the digital image correlation [6]

2.2.2 Tensile Tests

Standard tensile tests (e.g. ISO 6892-1) are used to determine the normal elastic moduli, the tension strengths, and Poisson's ratios.

A normalised specimen (Fig. 10) is inserted into a tensile testing machine and fixed. The tensile load is gradually increased until rupture occurs. The loading data are obtained directly from the loading machine. Different approaches for strain measurement exist. In the quoted tests, DIC was used to measure the strains. Elastic moduli and tensile strength are taken from the stress-strain curve while the Poisson's ratios are computed from only the DIC. [4]

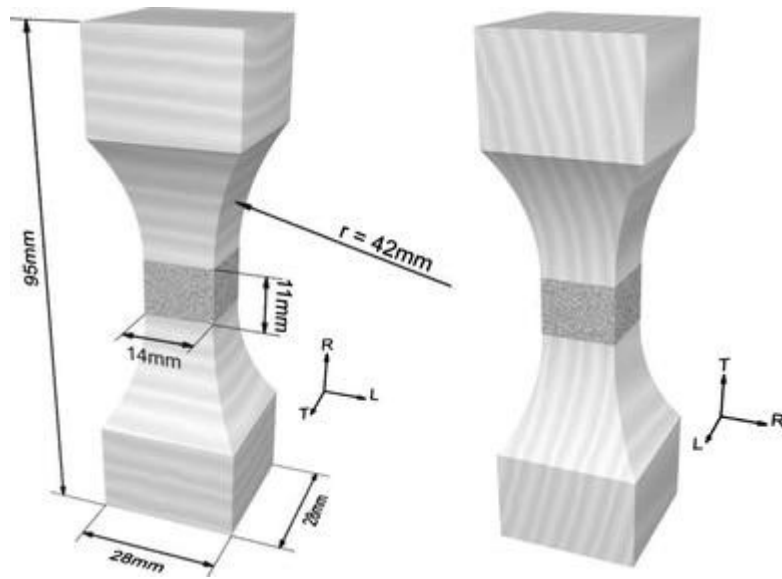


Fig. 10 - The specimen used for the tensile test [4]

2.2.3 Compression Tests

The basic principle of a compression test is the same as that of the tensile test, but compressive stress is applied instead of tensile stress. Fig. 11 illustrates compression test set-up. The stress-strain curve of compressive tests does not show an unequivocal point of rupture, so it is evaluated optically. [7]

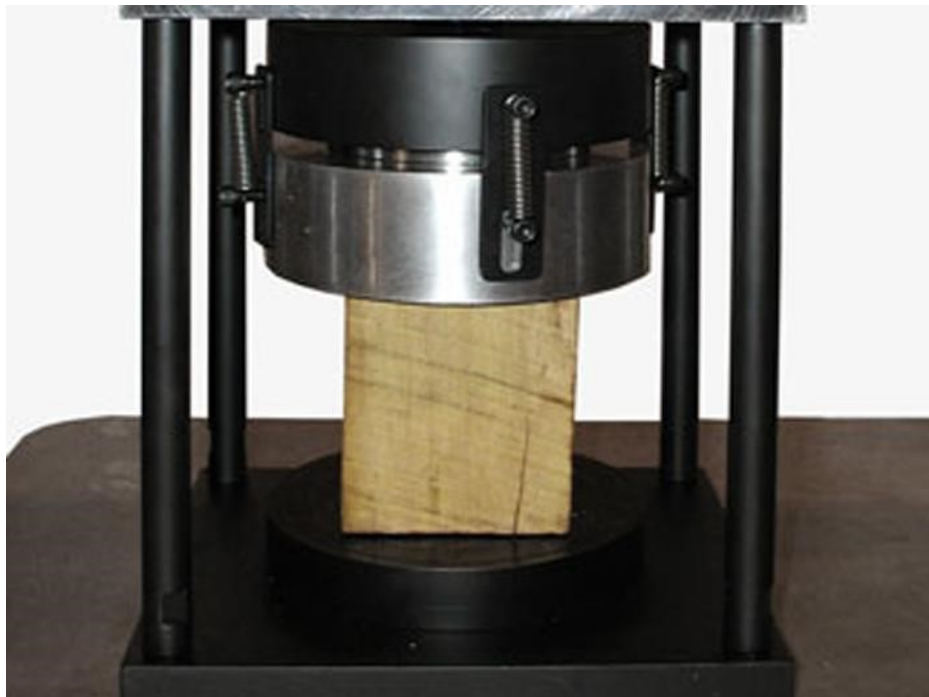


Fig. 11 - The compressive test set-up - an illustrative image [8]

Fig. 12 shows stress-strain curves in tangential and radial direction with different MC in compression.

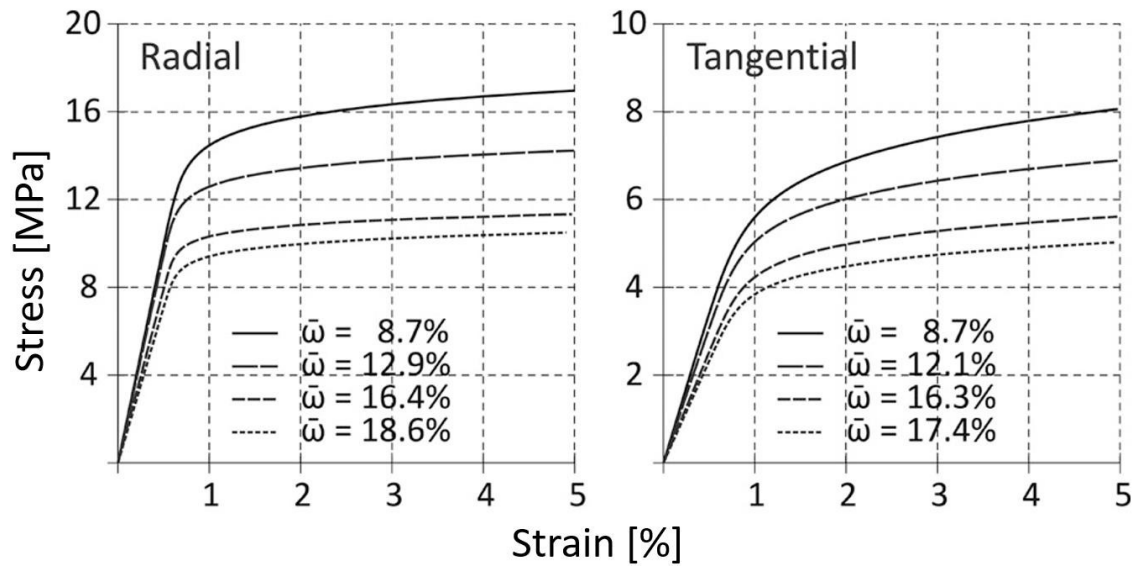


Fig. 12 - Stress-strain curves at different MC of European beech wood in compression in radial (left) and tangential (right) direction [7]

2.2.4 Torsion Test

The torsion testing machine consists of a static jaw and a rotary jaw. The specimen is fixed to the machine and rotated until rupture. The torsion test is used to measure shear strength in the longitudinal direction and an apparent shear modulus. The experimental set-up is shown in Fig. 13.

The apparent shear modulus is according to [9] calculated as:

$$G_a = \frac{M}{\theta J}, \quad (3)$$

where M is the applied torque, J is the quadratic cross-sectional moment of inertia, and θ is the torsion angle per unit length.

From its definition, the apparent shear modulus is the average of the two longitudinal shear moduli: $G_a = \frac{G_{LR} + G_{LT}}{2}$.

The shear moduli are then calculated according to the theoretical and experimental distribution of the shear strain. [5]

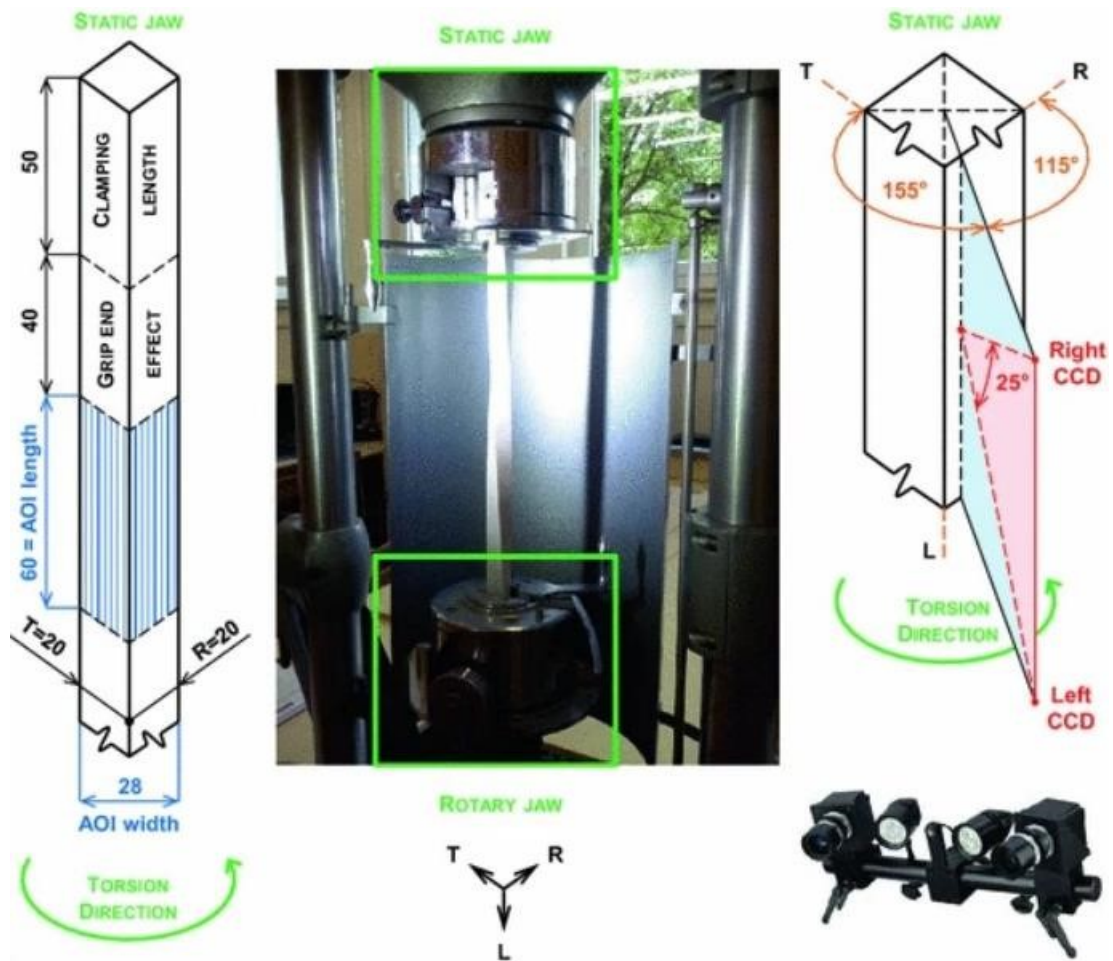


Fig. 13 - The torsion test set-up [5]

2.2.5 A Special Shear Testing Method

A specifically designed testing method was used for shear properties testing in [10]. Fig. 14 shows the test set-up, the sample shape, and the deformation of the measuring field. The shear frame is loaded and deformed by pure shear loads, which are transferred to the specimen. Specimens of variable thickness were used and loaded until rupture occurred. The testing method is described in more detail in [10]

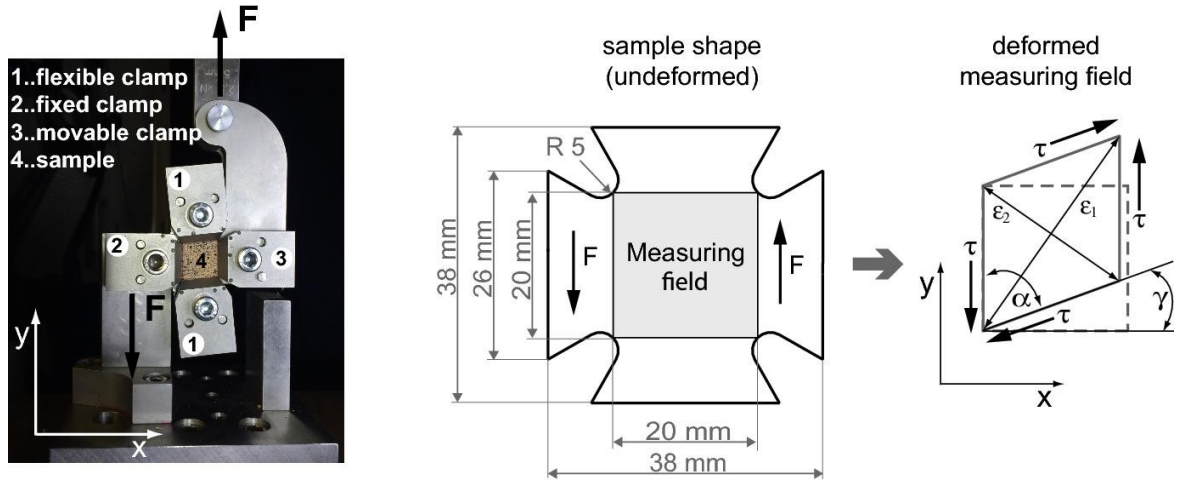


Fig. 14 - The test set-up (left), the sample (middle) and the deformation of the measuring field (right) [10]

2.2.6 Ultrasonic Wave Utilization

Another new testing method is using ultrasonic waves to determine the elastic characteristics. At least three wave propagation velocities in each the normal, shear and quasi-shear directions are needed to determine all orthotropic elastic properties.

For orthotropic materials, the stiffness matrix \mathbf{C} is formed as:

$$\mathbf{C} = \begin{pmatrix} c_{11} & c_{12} & c_{13} & 0 & 0 & 0 \\ c_{12} & c_{22} & c_{23} & 0 & 0 & 0 \\ c_{13} & c_{23} & c_{33} & 0 & 0 & 0 \\ 0 & 0 & 0 & c_{44} & 0 & 0 \\ 0 & 0 & 0 & 0 & c_{55} & 0 \\ 0 & 0 & 0 & 0 & 0 & c_{66} \end{pmatrix} \quad (4)$$

The compliance matrix \mathbf{S} :

$$\mathbf{S} = \mathbf{C}^{-1} = \begin{pmatrix} 1/E_1 & -\nu_{12}/E_2 & -\nu_{13}/E_3 & 0 & 0 & 0 \\ -\nu_{21}/E_1 & 1/E_2 & -\nu_{23}/E_3 & 0 & 0 & 0 \\ -\nu_{31}/E_1 & -\nu_{32}/E_2 & 1/E_3 & 0 & 0 & 0 \\ 0 & 0 & 0 & 1/G_{23} & 0 & 0 \\ 0 & 0 & 0 & 0 & 1/G_{13} & 0 \\ 0 & 0 & 0 & 0 & 0 & 1/G_{12} \end{pmatrix} \quad (5)$$

The elastic coefficients of the stiffness matrix were calculated from the following equations [2]:

$$c_{11} = \rho V_{LL}^2 \quad (6)$$

$$c_{22} = \rho V_{RR}^2 \quad (7)$$

$$c_{33} = \rho V_{TT}^2 \quad (8)$$

$$c_{44} = (\rho V_{TR}^2 + \rho V_{RT}^2)/2 \quad (9)$$

$$c_{55} = (\rho V_{LT}^2 + \rho V_{TL}^2)/2 \quad (10)$$

$$c_{66} = (\rho V_{LR}^2 + \rho V_{RL}^2)/2 \quad (11)$$

$$c_{23} = \sqrt{(c_{22} + c_{44} - 2\rho V_{RT/RT}^2)(c_{33} + c_{44} - 2\rho V_{RT/RT}^2)} - c_{44} \quad (12)$$

$$c_{13} = \sqrt{(c_{11} + c_{55} - 2\rho V_{LT/LT}^2)(c_{33} + c_{55} - 2\rho V_{LT/LT}^2)} - c_{55} \quad (13)$$

$$c_{12} = \sqrt{(c_{11} + c_{66} - 2\rho V_{LR/LR}^2)(c_{22} + c_{66} - 2\rho V_{LR/LR}^2)} - c_{66} \quad (14)$$

Where ρ is density and V_{11} , V_{12} and $V_{12/12}$ are the wave propagation velocities in normal, shear and quasi-shear directions, respectively.

The testing method is described in further detail in [2]

While the method proved useful for the elastic moduli determination, the values of the Poisson's ratios were most likely incorrect due to the false premise of perfect elastic orthotropic symmetry.

2.3 Wood Failure Simulation in LS-DYNA

The FEM solver LS-DYNA offers over 300 different material models, including the model MAT_WOOD, which is designed to fit the properties of various types of wood.

Southern yellow pine and Douglas fir are predefined and can be activated by material model options, while other wood types including European beech require complete data input. [11]

2.3.1 Material Model

Wood is generally assumed to be orthotropic, having different properties in three mutually perpendicular directions – longitudinal, tangential, and radial. LS-DYNA simplifies the orthotropic material model to a transversely isotropic model not differentiating between radial and tangential directions. Often, the longitudinal direction is referred to as the parallel direction and the radial and tangential directions are referred to as the perpendicular direction. The orthotropic and the transversely isotropic material models are compared in Fig. 15.

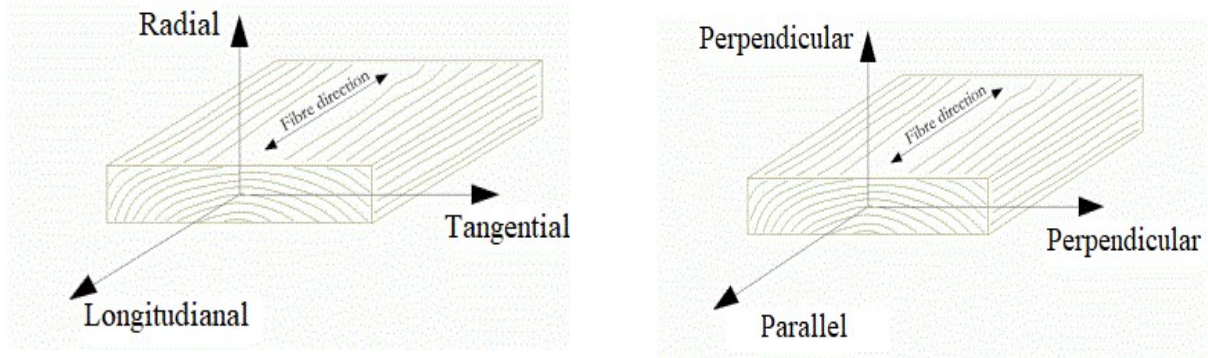


Fig. 15. Comparison of an orthotropic (left) and a transversely isotropic (right) model of wood [3]

2.3.2 Elastic Properties

The transversely isotropic material model requires five independent elastic constants: Two normal modules (E_L and E_T), two shear modules (G_{LT} and G_{TR}) and the major Poisson's ratio (ν_{LT}). The other two Poisson's ratios are dependent on the five constants and are computed internally as:

$$\nu_{TL} = \nu_{LT} \left(\frac{E_T}{E_L} \right) \quad (15)$$

$$\nu_{TR} = \frac{E_T - 2 \cdot G_{TR}}{2 \cdot G_{TR}} \quad (16)$$

2.3.3 Failure Criteria

Modelling failure of orthotropic or transversely isotropic materials is complicated compared to isotropic materials. Principal stresses lie in general directions most of the time and therefore they are not used to describe failure. Instead, not only normal load but also shear needs to be considered. Various approaches for failure exist - non-interactive criteria, interactive criteria, and direct mode criteria. Different sets of coefficients are required for different approaches.

Non-interactive criteria also referred to as limit criteria are the simplest, comparing each load individually with the corresponding strength. Non-interactive criteria include maximum stress criteria and maximum strain criteria. Failure occurs when any of these inequalities are violated:

Maximum stress	Maximum strain
$-X_C < \sigma_L < X_T$	$-X_{\varepsilon C} < \varepsilon_L < X_{\varepsilon T}$
$-Y_C < \sigma_T < Y_T$	$-Y_{\varepsilon C} < \varepsilon_T < Y_{\varepsilon T}$
$-S_{LT} < \sigma_{LT} < S_{LT}$	$-S_{\gamma LT} < \gamma_{LT} < S_{\gamma LT}$
$-S_{TR} < \sigma_{TR} < S_{TR}$	$-S_{\gamma TR} < \gamma_{TR} < S_{\gamma TR}$

X , Y and S are the stress or strain limits for normal loads in parallel and perpendicular direction, and shear load respectively; σ is stress and ε and γ are normal and shear strains. The indexes C and T indicate compressive or tensile load. The indexes LT and TR indicate the shear planes.

The interactive criteria take into account that the individual loads are mutually weakening. More complex equations are used to describe failure. Various interactive criteria exist with different levels of simplification. Those include Tsai-Hill criterion, Hoffmann criterion, or Tsai-Wu criterion.

Direct mode criteria also consider interactions between the loads. Above that, they distinguish modes of material failure. Direct mode criteria can be highly complex and provide very realistic results, like the LaRC criteria. Direct mode criteria also include Puck criteria, Hashin criteria, or Modified Hashin criteria. [12]

The Hashin criteria distinguishes the following four modes of damage:

The tensile fibre damage ($\sigma_L \geq 0$):

$$\left(\frac{\sigma_L}{X_T}\right)^2 + \frac{\sigma_{LT}^2}{(S_{TR})^2} \geq 1 \quad (17)$$

The compressive fibre damage ($\sigma_L < 0$):

$$\left(\frac{\sigma_L}{X_C}\right)^2 \geq 1 \quad (18)$$

The tensile matrix damage ($\sigma_T > 0$):

$$\left(\frac{\sigma_T}{Y_T}\right)^2 + \frac{\sigma_{LT}^2}{(S_{TR})^2} \geq 1 \quad (19)$$

The compressive matrix damage ($\sigma_T < 0$):

$$\left[\left(\frac{Y_C}{2 \cdot S_{LT}}\right) - 1\right] \left(\frac{\sigma_T}{Y_C}\right) + \left(\frac{\sigma_T}{2 \cdot S_{LT}}\right)^2 + \left(\frac{\sigma_{LT}}{S_{TR}}\right)^2 \geq 1 \quad (20)$$

In the Modified Hashin criteria it is assumed that shear stress weakens the material in compression as well as tension. The failure criteria have slightly modified form:

The tensile and compressive fibre damage:

$$\left(\frac{\sigma_L}{X}\right)^2 + \frac{\sigma_{LT}^2 + \sigma_{LR}^2}{S_{TR}^2} \geq 1 \quad X = \begin{cases} X_T \text{ for } \sigma_L > 0 \\ X_C \text{ for } \sigma_L < 0 \end{cases} \quad (21)$$

The tensile and compressive matrix damage:

$$\frac{(\sigma_T + \sigma_R)^2}{Y^2} + \frac{(\sigma_{TR}^2 - \sigma_T \cdot \sigma_R)}{S_{LT}^2} + \frac{(\sigma_{LT}^2 + \sigma_{LR}^2)}{S_{LT}^2} \geq 1 \quad X = \begin{cases} Y_T \text{ for } \sigma_{22} + \sigma_{33} > 0 \\ Y_C \text{ for } \sigma_{22} + \sigma_{33} < 0 \end{cases} \quad (22)$$

A reduced form of Modified Hashin is used to describe failure in LS Dyna and is discussed further in [11].

2.4 Basics of the Mathematics Behind the Explicit and Implicit Finite Element Method Computations

The finite element method (FEM) is a numerical method of solving various engineering problems as static or dynamic response of elastic bodies. It works on the principle of subdividing a complex, practically incomputable unit, into smaller parts called elements. The displacement of an element is interpolated from the values in its nodes. Mechanical properties of the material need to be added to form the stiffness matrix K , the damping matrix C , or the mass matrix M . The behaviour of the elements and nodes is described by the equation:

$$M\ddot{x} + C\dot{x} + K\Delta x - P = 0 \quad (23)$$

In which P is the body force and external load vector and x is the coordinate vector.

Either explicit or implicit method is used to solve the partial differential equation. [13]

2.4.1 Explicit simulations

The explicit simulation method is the simpler of the two methods expressing each state as a function of the previous one:

$$x_{n+1} = f(x_n, \dots) \quad (24)$$

This approach implies that the inaccuracies accumulate with each time step, thus diverging from the correct value. [14]

The time step size is limited by the Courant–Friedrichs–Lewy condition which says that the time step must be smaller, than the time necessary for a wave to travel between any of the adjacent nodes. The condition is represented by the equation:

$$\Delta t_{max} = \frac{d_{min}}{c}, \quad (25)$$

where Δt is the maximum possible time step, d_{min} is the smallest distance between two adjacent nodes and c is the speed of sound in the material which is defined as:

$$c = \sqrt{\frac{E}{\rho(1 - \nu)}}, \quad (26)$$

where E is the normal elastic modulus, ρ is the density and ν is the Poisson's ratio of the material.

The explicit method is a fast, efficient method that calculates the time integration solution directly.

2.4.2 Implicit simulations

In the implicit simulation method, the current state cannot be directly (or “explicitly”) expressed as a function of the previous state. It uses the previous state as well as the current state to compute the current state iteratively, thus requiring convergence.

It typically requires 100 to 10000 fewer time steps than explicit. The problem is that the cost of each time step is unpredictable since it depends on the convergence behaviour of the simulation.

The implicit method divides to implicit static and implicit dynamic. Generally, implicit static is a significant advantage of the implicit method for the possibility to neglect all dynamic effects. However, dynamic effects are expected to play an important role and need to be considered in simulations of this specific experiment.

The convergence of the FEM simulation is significantly influenced by the condition number, which describes the rate of change in output caused by a small change in the input of a function. The condition number is among other things increased by increasing the number of parts included in the FEM simulation. The number of boundaries and constraints decreases the condition number.

Formation of a relatively large amount of chips with no boundaries or constraints increases the condition number critically. [13]

3 Experiment

A specialized experiment to measure the cutting forces on a single chainsaw tooth was developed in STIHL. The experiment is set up to simulate the conditions of chainsaw cutting as authentically as possible. In addition to the provided data, a different interpretation of the forces is covered in chapter 3.4.

3.1 Setup

A cylinder-shaped European beech wood is turned by a single incisor. The initial diameter of the wood is 150 mm. In the data from the experiment, it is said that the wood is saturated with MC 55 % [15]. It is striking, that the value should be this high since no data for MC higher than 19 % was found in the literature. In the LS Dyna manual, values from 23 % to 30% MC are stated for saturated wood. The values from the manual seem more realistic.

A custom made three jaw chuck is used to hold the wood. The incisor is a tooth from a serial saw chain from STIHL marked 3/8" RS (Fig. 16). The incisor is attached to a turning tool, which is optimized for this experiment. The head of the tool is designed to hold the incisor. The body of the tool has grooves to lead the wiring of strain gauges, which are used as one of the means of the cutting forces measurement. The other device measuring the cutting forces is a load cell holding the turning tool.



Fig. 16 - The incisor

The rotation of the wood is accelerated during the simulation to maintain a constant cutting speed of 16.67 m/s. The feed rate is 0.3 mm/U or approximately 12.6 mm/s (the speed must be increased as the rotation accelerates to maintain the feed rate 0.3 mm/U).

The experiment setup is shown in Fig. 17.

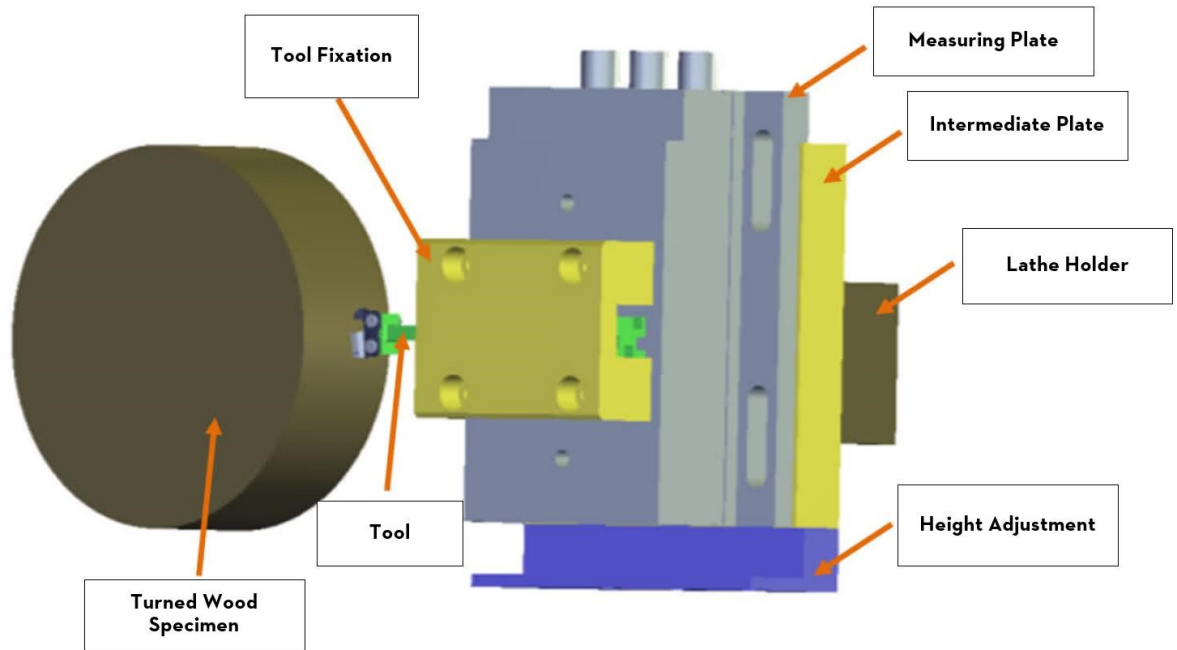
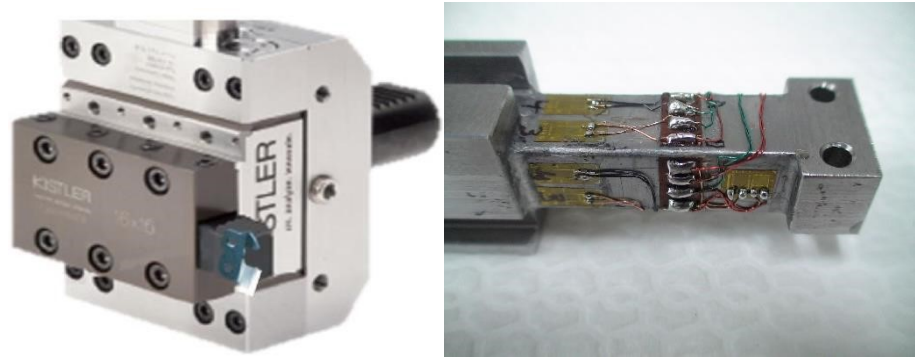


Fig. 17 - The experiment setup

3.2 Measurements

Seven experiments were carried out with this setup, each measuring with both the load cell and the strain gauges which are both further referred to as “the measuring systems” (Fig. 18), giving a total of 14 measurement data in each x, y, and z axis. The data were measured at a sampling rate of 10,000 Hz. A measurement takes approximately 2-4 seconds, which results in up to 40,000 values per axis and measuring system. The measuring systems were calibrated with forces at the tip of the incisor while connected to a computer which calculates the forces internally.



a) The load cell holding the tool b) The tool with the strain gauges

Fig. 18 - The measuring systems

The system was recorded by a highspeed camera and a GoPro for the evaluation of the chip formation. A sample photo from the highspeed camera recording can be seen in Fig. 19.

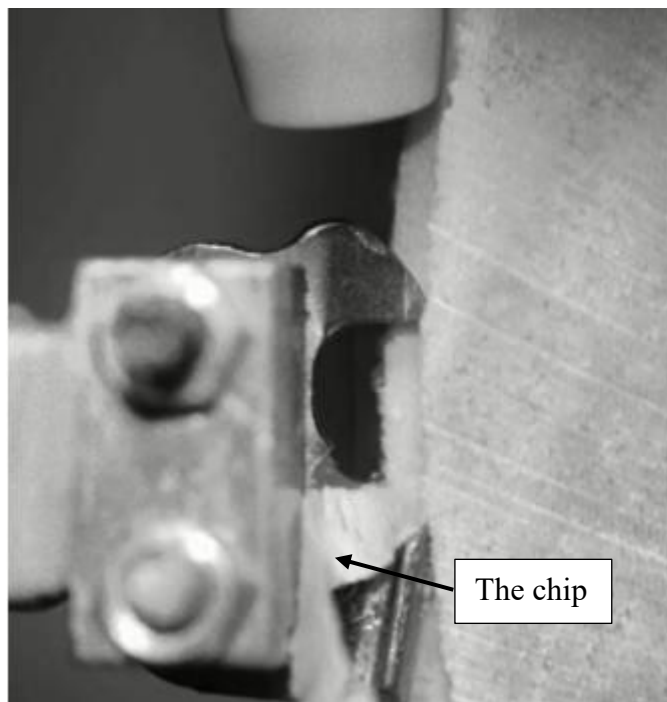


Fig. 19 - A sample photo from the highspeed camera recording

3.3 Evaluation

The measurement data contains large peaks and valleys (the direction of the forces in the peaks and valleys is opposite for almost every measurement for both measuring systems and

all axes). An envelope was created giving the maximal and minimal forces and also a mean value curve was created reducing the data volume to 254 points on each curve.

Vibrations are the most probable cause of the peaks and valleys this big. The inhomogeneity of the wood can influence the vibrations significantly. Therefore, the mean value curve is used as reference for comparison with the numerical simulation.

3.4 Results

Even though [15] suggests calibrating the FEM simulation to match the mean values of the peak forces to present the worst-case scenario, the aim of this simulation is not to determine whether the incisor could be damaged, but rather to measure the effectivity of the incisor geometry, so the effect of the peaks of the forces does not have to be taken into consideration.

The specific results could not be revealed, as they are a property of the Stihl company. The graphs and the proportions, however, are not classified and can be shown and discussed. The values on the graphs were normalized.

A mean value is calculated for each measurement on the time interval, in which the incisor is clearly fully engaged. Since the point of engagement is different for each measurement, the time interval is individual. In each direction, the minimum and maximum mean values are compared for each measuring system. The overall minimal and maximal mean values are also compared for each direction. The coordinate system is shown in Fig. 20.

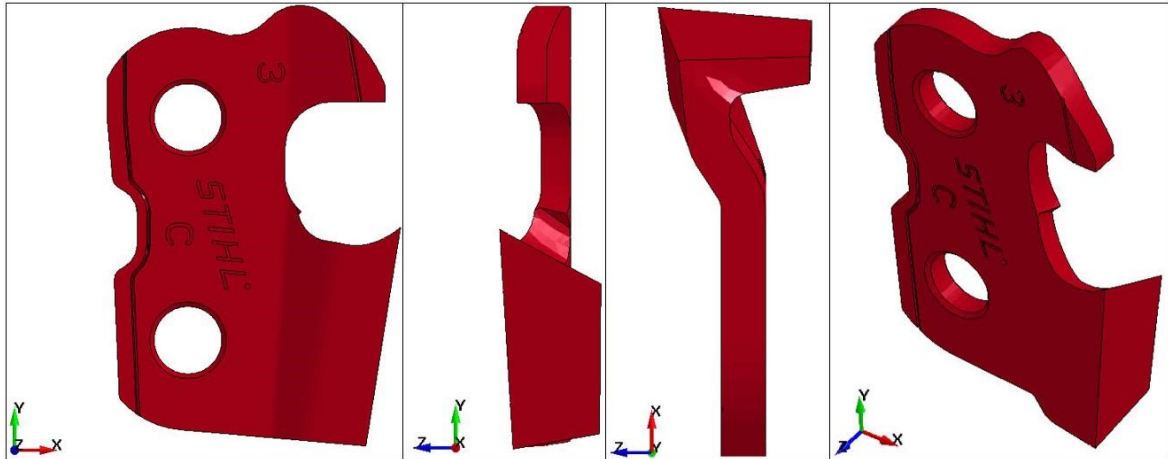
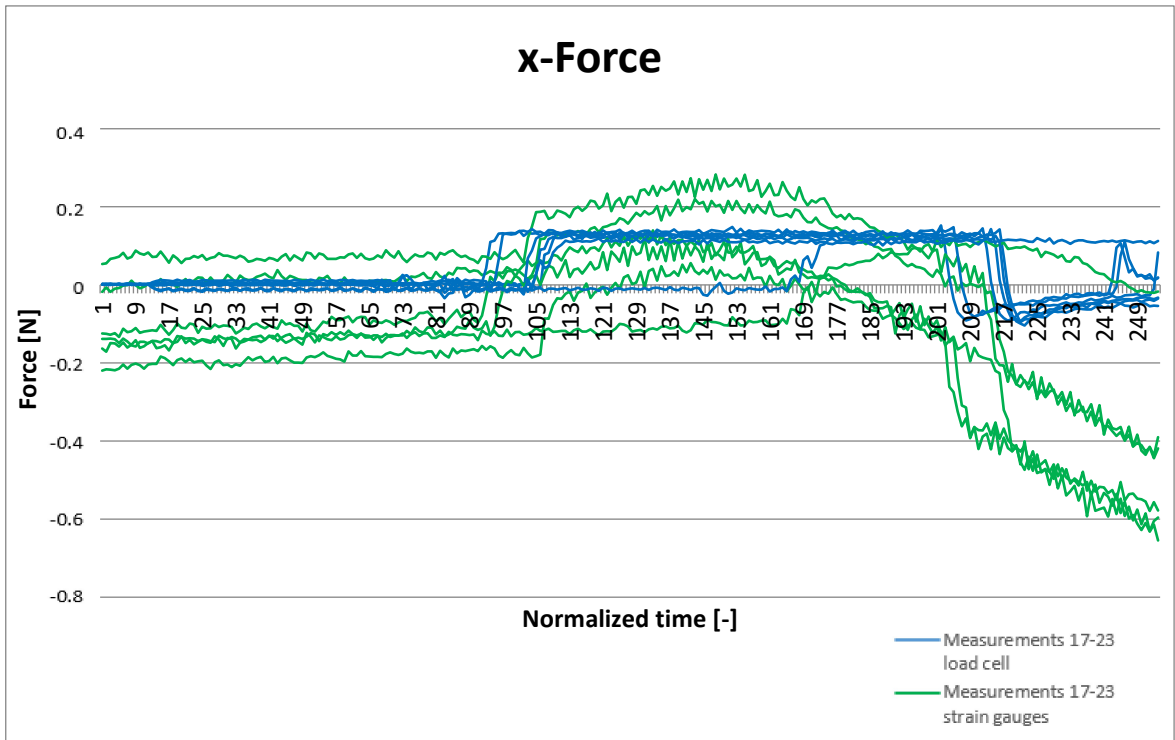


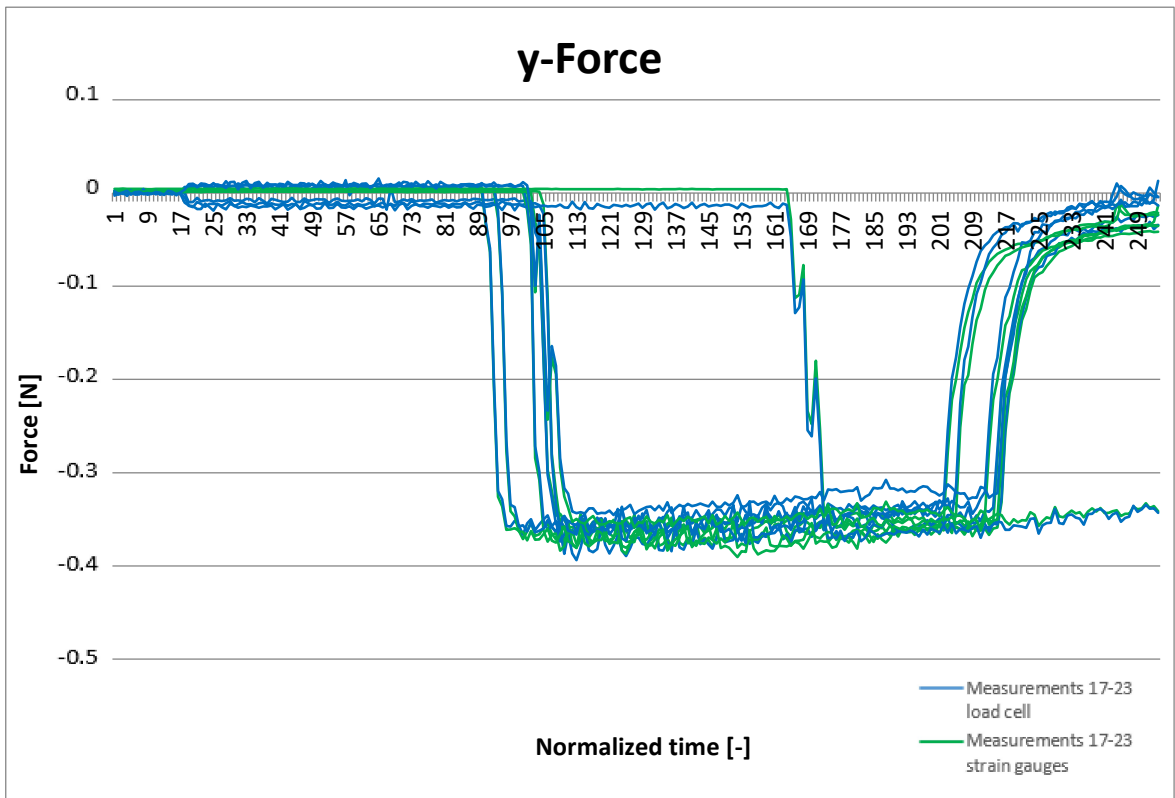
Fig. 20 - Coordinate system of the incisor

Experiments with different setups were also carried out so the measurements are numbered from 17 to 23. The other setups are not examined in this thesis.

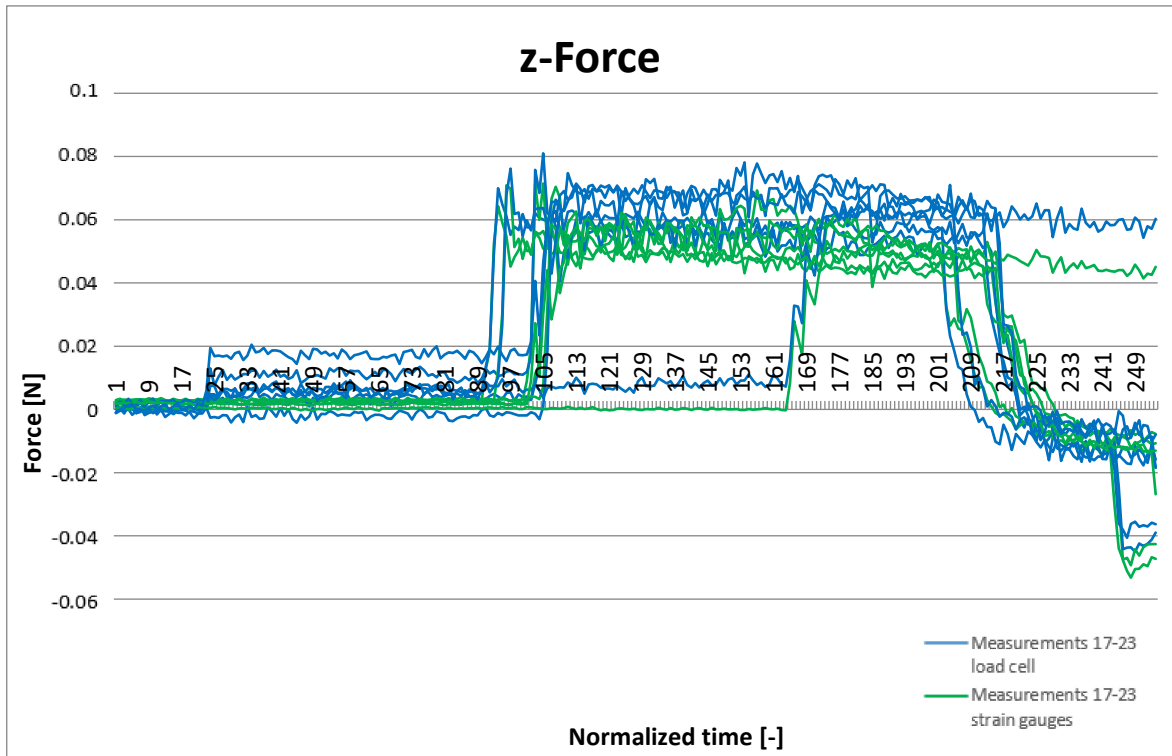
Most of the mean value curves fluctuate around a nearly constant value when the incisor is engaged. The only exception is the x-force measured by the strain gauges, which is very unstable and gives inconsistent results. The reason for this could be wrong connection of the strain gauges or bad calibration since the mean value curves do not start at zero. The data from the strain gauges for the x direction are assumed to be wrong and are not considered further. The data from the strain gauges (green) and the load cell (blue) are compared for each direction (Fig. 21). The unstable behaviour of the x-force data measured by the strain gauges can be seen in Fig. 21 a). The forces are scaled by the same factor in the thesis in order not to reveal confidential data. For each measurement 254 force values were provided to us with no time step assigned. Since the duration of the measurements is inconsistent, the time scale (x axis of the graph) is normalized.



a) *The x-force*



b) *The y-force*



c) The z-force

Fig. 21 - Forces from the strain gauges (green) and the load cell (blue)

Directions y and z show slight decrease in the course of the simulation. The most probable explanation is that, as the diameter of the wood decreases during the simulation, the conditions of the cutting are slightly changed. All directions are summarized in Table 1.

Table 1 – The maximal and minimal forces in each direction (normalized)

	SG_{min}	SG_{max}	LC_{min}	LC_{max}	$\frac{SG_{max}}{SG_{min}}$	$\frac{LC_{max}}{LC_{min}}$	$\frac{max}{min}$
x	N/A	N/A	0.11036	0.13568	N/A	1.2294	1.2294
y	0.34731	0.37143	0.32859	0.36640	1.0694	1.1151	1.1304
z	0.04634	0.05774	0.05436	0.06783	1.2459	1.2477	1.4636

In the x direction, the difference between the minimal and maximal value is 22.94 %. The difference is relatively high, given that only data from the load cell are used and the data from the strain gauges are not evaluated and will not be compared with the FEM simulation.

The difference in the y direction is lower (13.04 %), even though values from different measuring systems are compared. The reason for this may be the fact that the absolute values of the y-force are significantly higher.

The difference in the z-force is the highest (46.36 %). This is not surprising since the z-forces are by far the lowest.

The FEM simulation will be calibrated to match the values as closely as possible.

4 Investigation of the Sensitivity of the Numerical Simulations on Individual Parameters

In this chapter, several parameters were varied and the effect on the chip and the cutting forces was observed. The sensitivity was analysed using a simplified model in order to lower the computation time.

4.1 Chip Formation

The first objective is to calibrate the simulation to form a realistic chip while using reasonable material parameters and simulation settings.

4.1.1 Version 1.00 – First Attempt

The first model consists of two parts: the incisor and the wood.

Model

For simplification, a translative relative motion between the incisor and the wood is simulated, instead of the rotation. Since the experiment is set to imitate the conditions during chainsaw cutting (in which the relative motion is translative), the simplification is assumed reasonable.

For the calibration of the chip formation, more simplifications are implemented in order to reduce the computation time. The wood is replaced with a simple 0.6x25x8 block so only the tip of the incisor cuts 0.3 mm deep. The feed of the incisor is neglected.

The wooden block is meshed with 0.06x0.25x0.1 hexahedral elements. The hexahedral mesh is chosen because it provides the most accurate results and a block can be meshed with hexahedrons easily.

Tetrahedral mesh is chosen for the incisor because it is relatively simple to mesh complicated parts with them. The mesh size is 0.5 mm, with the tip of the incisor refined for a better contact with the wood. The meshes are shown in Fig. 22.

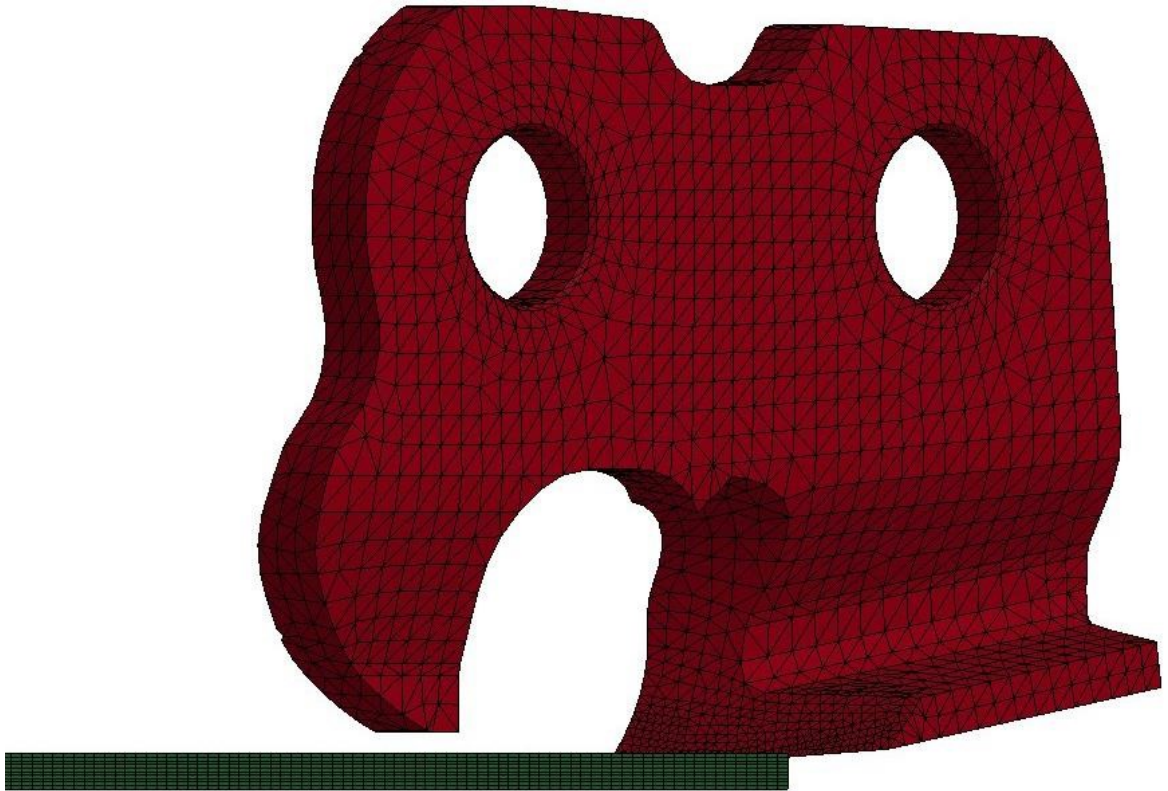


Fig. 22 - Meshes of the incisor and the wood

Two sets of nodes are used in this model. Set 1001 consist of the nodes on the upper surface of the wood. It is used for the velocity prescription. Set 5001 consist of all nodes of the wood and is used for the contact between the incisor and the wood.

All versions 1.XX are using this model or a similar model with the wood substituted by a block with different dimensions or mesh. The model is shown in Fig. 23.

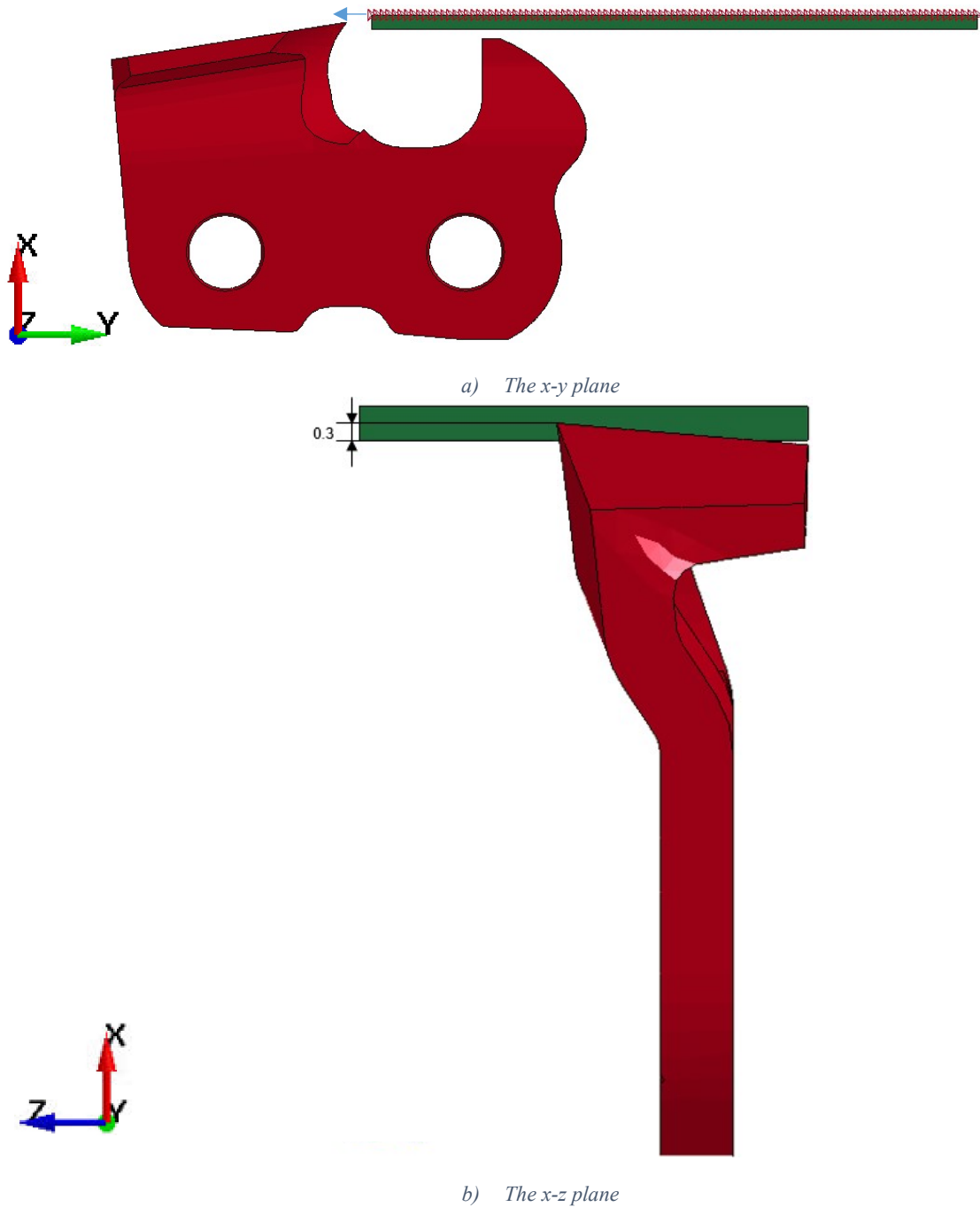


Fig. 23 - Version 1.XX model overview

Materials

The incisor is made of steel. The elastic moduli of steel are approximately two orders of magnitude larger than the elastic moduli of wood. For this reason, the incisor is modelled as a rigid body to simplify the model.

Card 1	1	2	3	4	5	6	7	8
Variable	MID	RO	NPLOT	ITERS	IRATE	GHARD	IFAIL	IVOL
Type	A8	F	I	I	I	F	I	I
Card 2	1	2	3	4	5	6	7	8
Variable	EL	ET	GLT	GTR	PR			
Type	F	F	F	F	F			
Card 3	1	2	3	4	5	6	7	8
Variable	XT	XC	YT	YC	SXY	SYZ		
Type	F	F	F	F	F	F		
Card 4	1	2	3	4	5	6	7	8
Variable	GF1I	GF2I	BFIT	DMAXI	GF1 \perp	GF2 \perp	DFIT	DMAX \perp
Type	F	F	F	F	F	F	F	F
Card 5	1	2	3	4	5	6	7	8
Variable	FLPAR	FLPARC	POWPAR	FLPER	FLPERC	POWPER		
Type	F	F	F	F	F	F		
Card 6	1	2	3	4	5	6	7	8
Variable	NPAR	CPAR	NPER	CPER				
Type	F	F	F	F				
Card 7	1	2	3	4	5	6	7	8
Variable	AOPT	MACF	BETA					
Type	F	I	F					
Card 8	1	2	3	4	5	6	7	8
Variable	XP	YP	ZP	A1	A2	A3		
Type	F	F	F	F	F	F		
Card 9	1	2	3	4	5	6	7	8
Variable	D1	D2	D3	V1	V2	V3		
Type	F	F	F	F	F	F		

Fig. 24 - Material cards of MAT_WOOD

The material model used is MAT_RIGID (MAT_20). The parameters input to the material model include density, Young's modulus, Poisson's ratio, and constraints. The elastic properties (Young's modulus and Poisson's ratio) must be input for contact analysis (choice of penalty).

Values $\rho = 7,850 \text{ kg} \cdot \text{m}^{-3}$, $E = 210,000 \text{ N} \cdot \text{mm}^{-2}$, and $\nu = 0.3$ are used. Translation and rotation are constrained in all directions.

The material model MAT_WOOD (MAT_143) is used for the wood. It is a complicated material model, with a lot of input parameters. The model offers two specific wood types:

Douglas fir (MAT_WOOD_FIR) and Southern yellow pine (MAT_WOOD_PINE). When those options are chosen, the number of input parameters is reduced significantly. The model offers no option for Beech wood, so all parameters must be chosen. The material card is shown in Fig. 24.

Card 1 contains an identification number, density, and parameters regarding plasticity and element failure principle. Card 2 contains elastic moduli and the Poisson's ratio ν_{LT} . Card 3 contains failure criteria. The parameters in Card 4 define the softening of the material and set the shape of the stress-strain curve. They are designed to reduce the mesh-size dependency. In Card 5, the strain rate dependency is defined. The parameters increase the strengths of wood as a function of strain rate. Card 6 contains the hardening parameters for modelling prepeak nonlinearity. Cards 7, 8, and 9 define the material axes of the transversely orthotropic material. The individual parameters are discussed more closely when they are varied.

An example model from the LS Dyna manual was used for the first model as a reference. The input parameters are shown in Fig. 25. The only difference in our material is that the flag IVOL was changed to 1. This allows the solver to invoke element erosion when negative volume occurs on them, instead of terminating the simulation.

```

$
*MAT_WOOD
$-->---1--->---2--->---3--->---4--->---5--->---6--->---7--->---8
$   mid|      ro|   nplot|   iters|   irate|   ghard|   ifail|   ivol|
      143 6.73E-10      0      0      0      0      0      1
$-->---1--->---2--->---3--->---4--->---5--->---6--->---7--->---8
$   el|      et|      glt|      gtr|      pr|
      11350      246.8      715.2      87.5      0.157
$-->---1--->---2--->---3--->---4--->---5--->---6--->---7--->---8
$   xt|      xc|      yt|      yc|      sxy|      syz|
      85.2      21.2      2.05      4.08      9.1      12.7
$-->---1--->---2--->---3--->---4--->---5--->---6--->---7--->---8
$   gf1|||  gf2|||  bfit|  dmax|||  gf1-||  gf2-||  dfit|  dmax-||
      42.7      88.3      30  0.99999  0.40  0.83      30  0.99
$-->---1--->---2--->---3--->---4--->---5--->---6--->---7--->---8
$   flpar|  flparc|  powpar|  flper|  flperc|  powper|
$-->---1--->---2--->---3--->---4--->---5--->---6--->---7--->---8
$   npar|  cpar|  nper|  cper|
      0.5  400.0  0.4  100.0
$-->---1--->---2--->---3--->---4--->---5--->---6--->---7--->---8
$   aopt|  macf|  beta|
      2      1
$-->---1--->---2--->---3--->---4--->---5--->---6--->---7--->---8
$   xp|  yp|  zp|  a1|  a2|  a3|
      0      1      0
$-->---1--->---2--->---3--->---4--->---5--->---6--->---7--->---8
$   d1|  d2|  d3|  v1|  v2|  v3|
      0      0      1

```

Fig. 25 - The slightly modified example material model

Element Formulation

The element formulation for the incisor is Type 13, which is a 1-point nodal pressure tetrahedron, a tetrahedron, with additional nodal averaging.

For the wood, the element formulation used is Type -2, which is a selective reduced (S/R) fully integrated solid intended for elements with poor aspect ratio, accurate formulation. From the AKKA company experience, this is the most stable and accurate element formulation for hexahedral elements. It also automatically switches the element topology to pentahedral element.

Timestep

There are several options to meet the Courant-Friedrichs-Lewy condition in LS-Dyna. One is to let the solver to automatically adjust the time step. This is the most accurate option. This option, however, is very computationally demanding. The other option is to prescribe a minimal time step strictly and adjust the material properties in order to increase the maximal time step. The method used in this model is mass scaling. The strictly prescribed time step for the first attempt is $1.75 \cdot 10^{-7}$ s, which is a commonly used time step in other simulations run in our company.

Contact

When materials with erosion are in contact, CONTACT_ERODING_... need to be used. CONTACT_ERODING_NODES_TO_SURFACE is the most stable one and is used for the first model. The contact is a function that every timestep checks the position of given nodes in relation of a given surface. When the nodes penetrate the surface (the nodes are on the other side of the surface), this function applies force proportional to the depth of the penetration, the material parameters, and the contact stiffness scale factor. The contact is defined between the surface of the incisor and the nodes of the wood (set 5001).

Contact settings standardly used in the AKKA company are used for this model with the friction coefficient set to 0.2. An additional keyword input card is added to define the contact for erosion.

Velocity prescription

The relative motion of the wood and the incisor is simulated by velocity prescription to the wood. In LS Dyna, all nodes and elements of all parts are static at the beginning of the simulation unless defined otherwise. If velocity prescription is applied to static entities, it is computed as if the entity accelerates to the desired velocity in a single time step. This could lead to simulation errors. For this reason, the keyword INITIAL_VELOCITY_GENERATION is used to define the wood at the beginning of the simulation as moving. To ensure that the wood is moving at a constant speed, the keyword BOUNDARY_PRESCRIBE_MOTION_SET is applied to a nodal set on the upper surface of the wood (set 1001). The prescribed velocity is $v_y = 16.67 \text{ m} \cdot \text{s}^{-1}$ which is the constant cutting speed maintained during the simulation.

Results

All elements in the path of the incisor are eroding, no chip is formed. Element erosion based on negative volume occurs in the simulation. The erosion of all elements could be caused by a mesh too coarse or a timestep too high. At the lowest point, the incisor cuts five element rows deep into the wood, so the mesh is considered as the less likely explanation. Also, a timestep too high is a common cause of negative volumes occurring in a simulation.

4.1.2 Version 1.01 – Timestep Decreased

Version 1.01 is the same as version 1.00, with the time step reduced to $4.0 \cdot 10^{-8}$ s.

Results

A chip is formed in this simulation. There are still imperfections on the chip. Still a large number of elements is eroding, and some elements are stretching through the incisor (Fig. 26). Since only the nodes are in contact with the incisor, the elements stretching through the incisor are not in conflict with the contact. However, the elements are still stretched in such a way, that is not physical (erosion should occur far sooner).

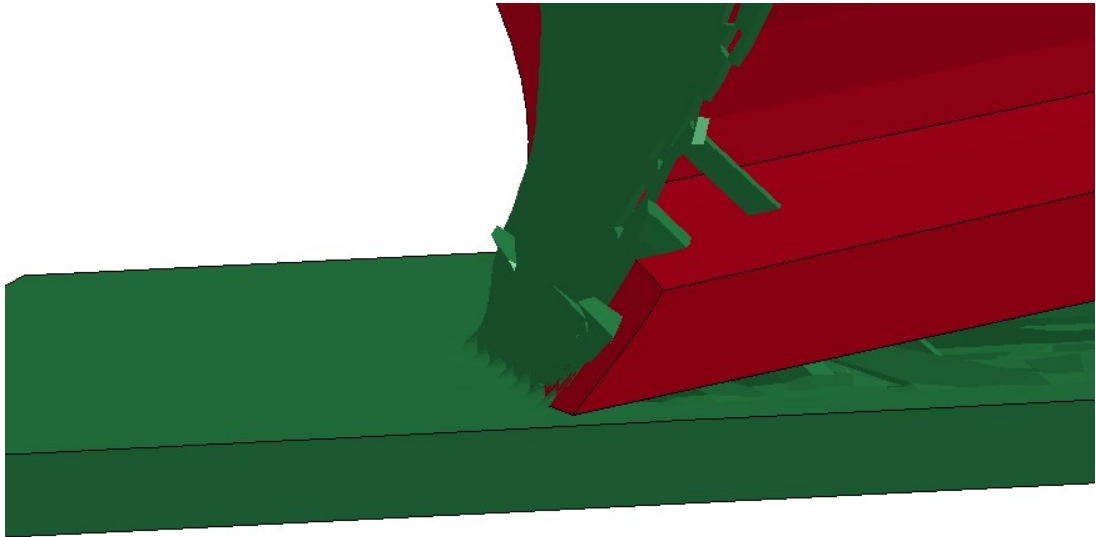


Fig. 26 - Unphysically stretched elements

The imperfections will be dealt with further. In the following step, the material data acquired from the literature were implemented to the model.

4.1.3 Version 1.02 – Material Data from the Literature

Based on the data from literature and suggestions given in the LS Dyna manual, a new material model is defined. Values from the middle of the ranges are picked for density and all Card 2 and Card 3 parameters. The softening parameters include uniaxial tensile, and pure shear fracture energies in parallel and perpendicular direction and other. The fracture energies are difficult to find in literature. A set of softening parameters for LS Dyna modeling of beech wood can be found in [16], although the way of calculating the energies

could be questioned. In further model versions, the fracture energies are searched in the range between the values from the example and the literature. In this version, all the softening parameters are taken from [16]. No data for the hardening parameters were found so the parameters from the example are left unchanged. In further versions the range suggested by the LS Dyna manual will be used. The material data are shown in Fig. 27.

```

$
*MAT_WOOD
$-->---1--->---2--->---3--->---4--->---5--->---6--->---7--->---8
$  mid|      ro|      nplot|    iters|    irate|    ghard|    ifail|    ivol|
   99902  0.67E-09      1      1      0      0      0      1
$-->---1--->---2--->---3--->---4--->---5--->---6--->---7--->---8
$  el|      et|      glt|      gtr|      pr|
   11000  1500      1000      400      0.05
$-->---1--->---2--->---3--->---4--->---5--->---6--->---7--->---8
$  xt|      xc|      yt|      yc|      sxy|      syz|
   100      50      5      10      10      14
$-->---1--->---2--->---3--->---4--->---5--->---6--->---7--->---8
$  gf1|||  gf2|||  bfit|  dmax|||  gf1-||  gf2-||  dfit|  dmax-||
   120      360      50  0.99999  0.6      1.8      50      0.99
$-->---1--->---2--->---3--->---4--->---5--->---6--->---7--->---8
$  flpar|  flparc|  powpar|  flper|  flperc|  powper|
$-->---1--->---2--->---3--->---4--->---5--->---6--->---7--->---8
$  npar|  cpar|  nper|  cper|
   0.5  400.0  0.4  100.0
$-->---1--->---2--->---3--->---4--->---5--->---6--->---7--->---8
$  aopt|  macf|  beta|
   2      1
$-->---1--->---2--->---3--->---4--->---5--->---6--->---7--->---8
$  xp|  yp|  zp|  a1|  a2|  a3|
      0      1      0
$-->---1--->---2--->---3--->---4--->---5--->---6--->---7--->---8
$  d1|  d2|  d3|  v1|  v2|  v3|
   0      0      1
$

```

Fig. 27 - Material card with parameters for beech wood – version 1.02

Results

Almost all elements of the wood erode at instance when the wood touches the incisor. The next step is to take the wood models from the versions 1.00 and 1.02 and combine the parameters to find out, which parameter or combination of parameters cause the erosion of the entire part.

4.1.4 Finding the Problem

A series of simulation was run with gradually substituting the parameters from the version 1.00 with the parameters from the version 1.02. It was found that the problem occurs when the elastic properties are substituted. Identical simulations with one having the perpendicular

Young's modulus (E_T) lowered closer to the example ($500 \text{ N} \cdot \text{mm}^{-2}$) and the other unchanged from the literature ($1500 \text{ N} \cdot \text{mm}^{-2}$), chip is formed in the first one, while in the second, the whole part erodes. With the bisection method, it was found that a simulation with $E_T = 1300 \text{ N} \cdot \text{mm}^{-2}$ forms a chip, $E_T = 1500 \text{ N} \cdot \text{mm}^{-2}$ erodes the whole model, and $E_T = 1400 \text{ N} \cdot \text{mm}^{-2}$ forms a very unnatural, very strangely behaving chip (Fig. 28). The values in the literature range from 420 to $2310 \text{ N} \cdot \text{mm}^{-2}$, with a significant difference between the E_T and the E_R value. The optimal value should not be at an edge of this interval. Since the parallel Young's modulus (E_L) used is higher than the perpendicular, the material models with higher E_T seem closer to an isotropic material model. Therefore, it is assumed that the high E_T is not the real problem or is a problem only with conjunction with other parameters, even though a chip is formed for realistic E_T values.

$E_T = 1400 \text{ N} \cdot \text{mm}^{-2}$ was chosen as a reference for finding other parameters causing the problem, because we should be able to observe a slight tilt towards either the chip formation or the erosion of the whole part. This reference version is marked 1.03.

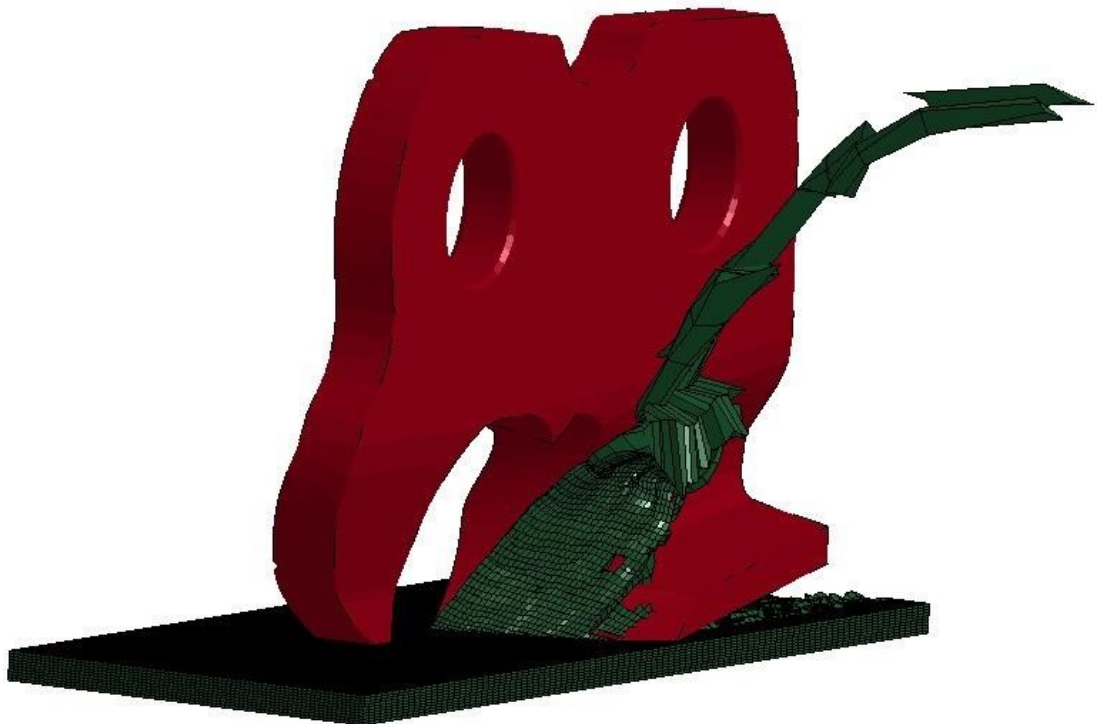


Fig. 28 - The strangely behaving chip

4.1.5 Element formulation

One of the things that would explain the unnatural behaviour of the chip would be the usage of a wrong element formulation for the wood. Type -2 formulation is considered the best for hexahedral elements with the only significant disadvantage being the computation power demand. This kind of simulation, however, is uncommon in the AKKA company. Therefore, the proper element formulation had to be sought for within this thesis from scratch. The principle in which the element formulation influences the model is overly complicated and is beyond the scope of this thesis. Other element formulations were tried empirically to see if an improvement could be reached. Types -1, 2, and 3 were used in the simulations.

Type -1 is a fully integrated S/R solid intended for elements with poor aspect ratio, efficient formulation. Regularly, this formulation gives slightly worse results and shorter computation time [17]. It is tried nevertheless, since this task is highly irregular, as mentioned earlier.

Type 2 is termed as a fully integrated S/R solid. In this formulation, there is a risk that shear locking could occur, if element aspect ratios are poor.

Type 3 is a fully integrated quadratic 8 node element with nodal rotations. It uses a different integration method than the other three.

Results

For all the newly tried element formulations, the result was worse than the original Type -2. Therefore, the idea of element formulation variation was refrained.

4.1.6 Poisson's Ratio

Since the problem is related to the elastic properties, one of the material properties investigated is the Poisson's ratio.

Values ranging from 0.04 to 0.05 were found in the literature for ν_{LT} and ν_{LR} , which are the lowest Poisson's ratio values of all directions. However, [11] implies that the ν_{LT} value should be greater than 0.1 and is about 10 times larger than ν_{TL} . A confusion between ν_{LT}

and ν_{TL} may have occurred since the standard order of the indexes is reverse in some countries. Values 0.14 and 0.4 were used in the simulations.

Results

The chip in the version with $\nu_{LT} = 0.14$ is similar to the one in version 1.03. With $\nu_{LT} = 0.4$ a change which could possibly be called an improvement is observed (Fig. 29). However, an objective comparison of the chips is not possible, and both the chips are in every way still far from a realistic one.

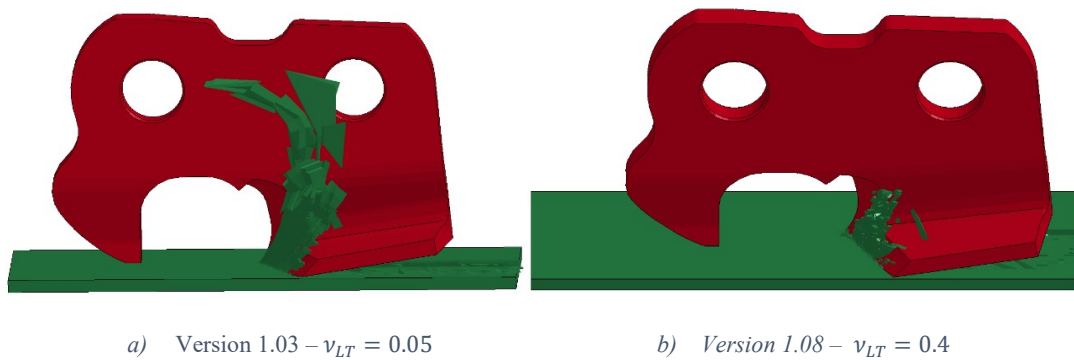


Fig. 29 - The chips with different Poisson's ratios

The ν_{TL} value is calculated internally in LS Dyna as:

$$\nu_{TL} = \nu_{LT} \cdot \frac{E_T}{E_L} \quad (15)$$

Therefore, the value 0.4 is used since values 0.04 to 0.05 could cause the ν_{TL} lower than 0.004.

4.1.7 Parallel Normal Modulus

Another elastic property investigated is the parallel normal modulus E_L . Since the problem is related to one of the normal moduli, it seems logical to investigate the other.

The normal moduli from the literature range from 8,200 to 13,700 N · mm⁻² and show some degree of moisture dependency, decreasing with higher MC. Therefore, the optimal value can also be searched lower than 8,200 N · mm⁻². Single values as high as 15,400 N ·

mm^{-2} [18] or even $17,000 \text{ N} \cdot \text{mm}^{-2}$ [16] were used in some simulations found in the literature.

The value was decreased and increased significantly, so that any influence of the normal modulus on the chip formation can be observed. Values $7,000 \text{ N} \cdot \text{mm}^{-2}$ and $16,000 \text{ N} \cdot \text{mm}^{-2}$ were used for the simulations.

Results

No considerable change in the chip formation was observed.

4.1.8 Version 1.11 – Perpendicular Shear Modulus

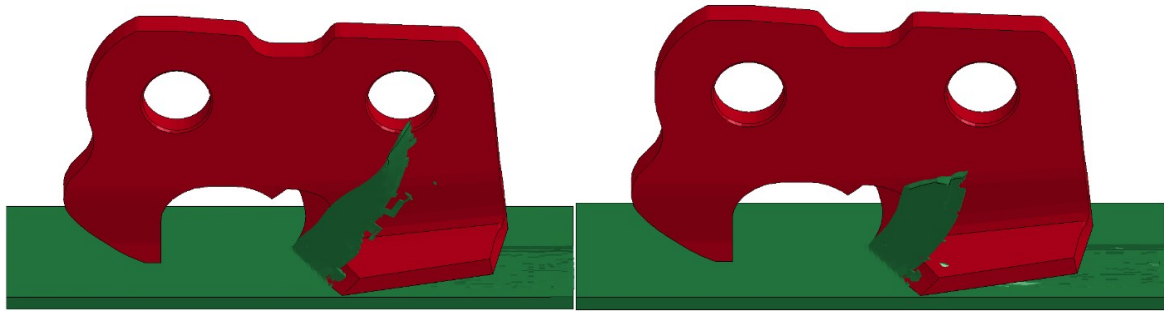
It is reasonable, that perpendicular shear modulus (G_{TR}) could influence the chip formation, since the perpendicular Poisson's ratio ν_{TR} is calculated internally by LS Dyna as:

$$\nu_{TR} = \frac{E_T - 2 \cdot G_{TR}}{G_{TR}} \quad (16)$$

For the version 1.03, the ratio is $\nu_{TR} = 0.75$. Even though values as high as 0.87 can be found in the literature, LS Dyna does not allow the user to input Poisson's ratios higher than 0.5 even for orthotropic materials. G_{TR} was changed to $500 \text{ N} \cdot \text{mm}^{-2}$ to reduce ν_{TR} to 0.4.

Results

The increase of G_{TR} and thus a reduction of ν_{TR} leads to the formation of a chip looking similarly to the one from version 1.01, with a lower number of elements eroding (Fig. 30). Still elements overly stretch through the incisor. The next step is to tackle this problem. This version of the simulation is taken as a reference.



a) *Version 1.01 – The reference material model* b) *Version 1.11 – The beech wood model*

Fig. 30 - Comparison of the chips from versions 1.01 and 1.04

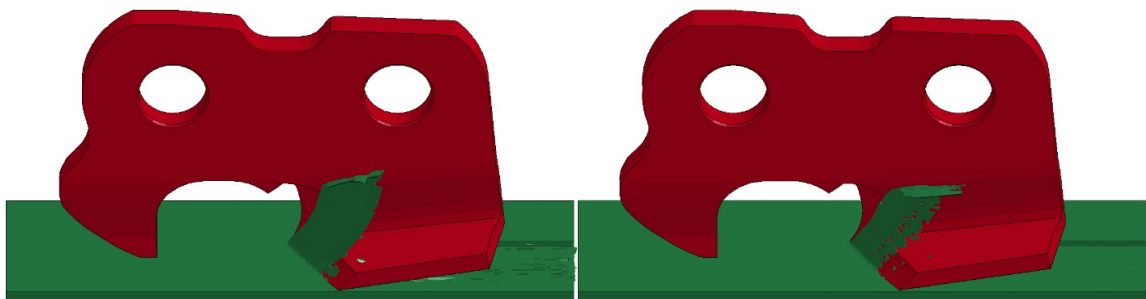
4.1.9 Version 1.12 – IFAIL on

The IFAIL flag in the first material card turns on and off erosion based on perpendicular damage.

The LS Dyna manual suggests using this flag only when excessive perpendicular damage causes computational difficulties. However, the types of simulations for which the material model is originally intended for differ from our simulation considerably. Erosion not allowed in a specific direction could explain the elements stretching far beyond the point, where failure would normally occur.

Results

The IFAIL flag solved the problem of the overly stretched elements. However, the flag also led to a considerable increase in the number of eroding elements. An increase was expected since a new means of erosion is allowed, but not an increase this high. The formed chip is shown in Fig. 31. The next step is to reduce the number of eroding elements.



a) *IFAIL = 0 (off)* b) *IFAIL = 1 (on)*

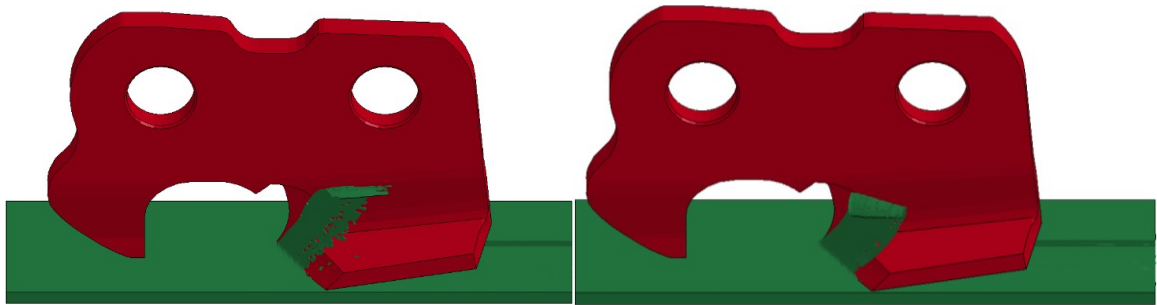
Fig. 31 - Comparison of the chip with erosion caused by perpendicular damage allowed

4.1.10 Version 1.13 – Timestep Further Decreased

The timestep is set to $2.0 \cdot 10^{-8}$ s. A further decrease of the timestep seems like the logical option, since the initial timestep decrease reduced the number of eroding elements significantly.

Results

In order to model a material failure, there is a minimal number of elements that must erode. With the timestep decreased, the minimal value seems to have been reached and the chip shape has been improved significantly (Fig. 32).



a) Version 1.12 – timestep = $4.0 \cdot 10^{-8}$ s

b) Version 1.13 – timestep = $2.0 \cdot 10^{-8}$ s

Fig. 32 - Comparison of the chips with different timesteps

The current shape of the chip is satisfactory. The next step is an investigation of the influence of single parameters on the cutting forces.

4.2 Contact Forces

The investigation of the influence of the parameters is done on a still very simplified model, so that a large number of simulations can be run. The varied parameters and the approximate increase or decrease of the cutting forces is summarized in Table 2. Version 2.01 is taken as a reference and other versions are compared with it.

Table 2 – Influence of individual parameters or set of parameters on the cutting forces

Varied parameter	Reference value	New value	x-force	y-force	z-force
Friction	0.3	0.2	+15 %	–10 %	+10 %
Wood thickness	0.6 mm	1.2 mm	<i>no effect</i>	<i>no effect</i>	<i>no effect</i>
Timestep	$2 \cdot 10^{-8}$ s	$4 \cdot 10^{-8}$ s	–40 %	–40 %	–50 %
Timestep	$2 \cdot 10^{-8}$ s	$1 \cdot 10^{-8}$ s	+10 %	+10 %	+10 %
Mesh x dimension	0.06 mm	0.12 mm	+10 %	+10 %	+20 %
Mesh x dimension	0.06 mm	0.03 mm	+20 %	+30 %	+15 %
Mesh y dimension	0.25 mm	0.125 mm	–15 %	–15 %	–20 %
Mesh z dimension	0.1 mm	0.2 mm	+15 %	+40 %	+40 %
Mesh z dimension	0.1 mm	0.05 mm	<i>no effect</i>	<i>no effect</i>	<i>no effect</i>
Contact definition	Nodes to surface	Surface to surface	–80 %	–50 %	–10 %
Contact scaling	1x	2x	<i>no effect</i>	<i>no effect</i>	<i>no effect</i>
Contact scaling	1x	4x	<i>no effect</i>	<i>no effect</i>	<i>no effect</i>
Elastic moduli	From version 1.11	Increased by 20 %	–10 %	–10 %	–20 %

Table 3 – Influence of individual parameters or set of parameters on the cutting forces – cont.

Varied parameter	Reference value	New value	x-force	y-force	z-force
Elastic moduli	From version 1.11	Decreased by ~20 %	+10 %	+10 %	+10 %
Failure criteria	From version 1.02	Increased by ~20 %	+20 %	+25 %	+30 %
Poisson's ratio	0.4	0.2	<i>no effect</i>	<i>no effect</i>	<i>no effect</i>
Poisson's ratio	0.4	0.05	<i>no effect</i>	<i>no effect</i>	<i>no effect</i>
Fracture energies	From [16]	From the material example	-35 %	-30 %	-40 %
B and D parameters	30	50	<i>no effect</i>	<i>no effect</i>	<i>no effect</i>
N parameters	$N_{ } = 0.3$ $N_{\perp} = 0.3$	$N_{ } = 0.4$ $N_{\perp} = 0.5$	<i>no effect</i>	<i>no effect</i>	<i>no effect</i>
c parameters	$c_{ } = 400$ $c_{\perp} = 100$	$c_{ } = 100$ $c_{\perp} = 100$	<i>no effect</i>	<i>no effect</i>	<i>no effect</i>
c parameters	$c_{ } = 400$ $c_{\perp} = 100$	$c_{ } = 1000$ $c_{\perp} = 1000$	+10 %	+10 %	+10 %
GHARD	0	0.02	-10 %	-10 %	-10 %

The investigation is described in more detail in chapters 4.2.1 to 4.2.12.

4.2.1 Version 2.00 – The First Model

For determining the dependence of single parameters on the cutting forces, a less simplified model is created. Whenever an increase or decrease is stated, it is meant in the sense of absolute values.

Model

The model is the same as the one from versions 1.XX, but translation in the x direction is allowed for the incisor, so that the feed can be prescribed. As the incisor moves in the x direction, the cutting depth slightly increases.

Velocity Prescription

In addition to the BOUNDARY_PRESCRIBED_MOTION_SET defining the movement of the wood, BOUNDARY_PRESCRIBED_MOTION_RIGID is added to define the x feed of the rigid incisor. Initial velocity is also prescribed to the incisor. The value of the prescribed velocity is $v_x = 12.6 \text{ mm} \cdot \text{s}^{-1}$.

Database

The only force acting on the cutting system is the force that the wood exerts on the incisor. It follows that the force transferred through the contact between the incisor and the wood should correspond with the overall force measured with the load cell and the strain gauges. In LS Dyna, there is a possibility to output the resultant forces that are transferred through a contact into an ASCII file or to a binary database. The keyword DATABASE_RCFORC is used.

Results

The master (incisor) x-force, y-force, and z-force values of the contact 5001 (Incisor_vs_Wood) are shown in a plot in Fig. 33.

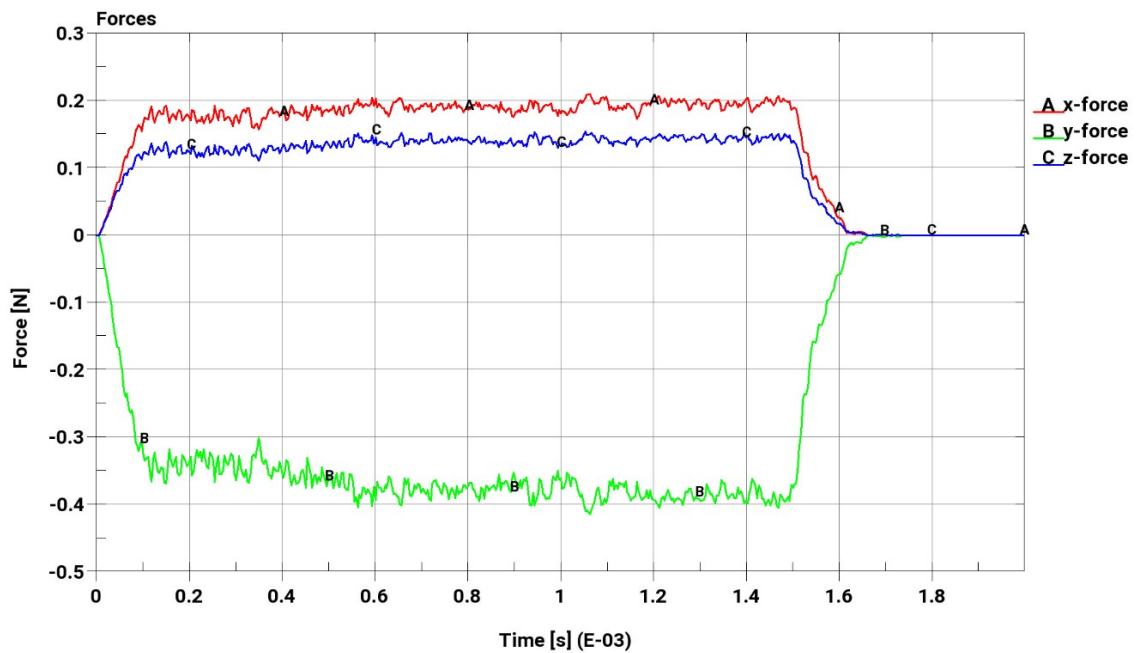


Fig. 33 - Contact forces in version 2.00

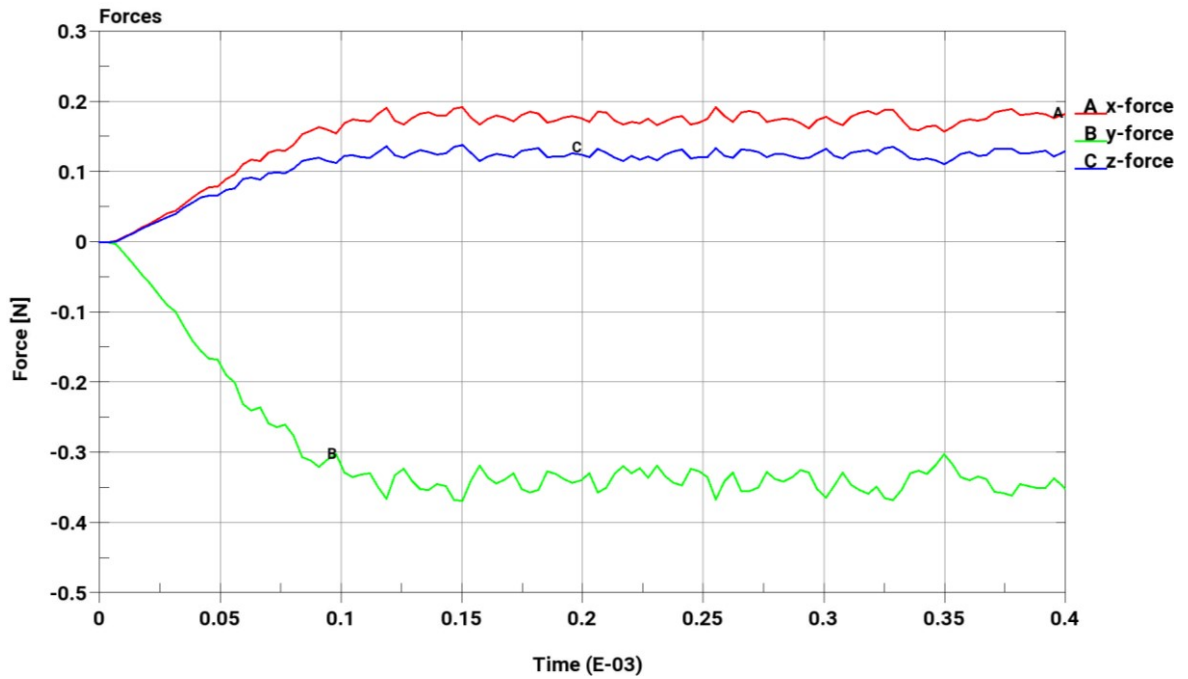
A slight increase can be seen in all the cutting forces during the simulation. The most probable explanation is the fact that the thickness of the chip increases as the incisor moves in the x direction. Fluctuations in the simulation are much smaller than in the experiment. While the fluctuations in the experiment are most likely caused by the inhomogeneity of the wood, the cause of the fluctuations in the simulation is most likely the step change in the forces related to element erosion. The values stabilize shortly after the engagement of the incisor. Therefore, the simulation can be terminated once stabilization is observed to decrease the computation time. This version is taken as a reference.

4.2.2 Version 2.01 – Friction Increased

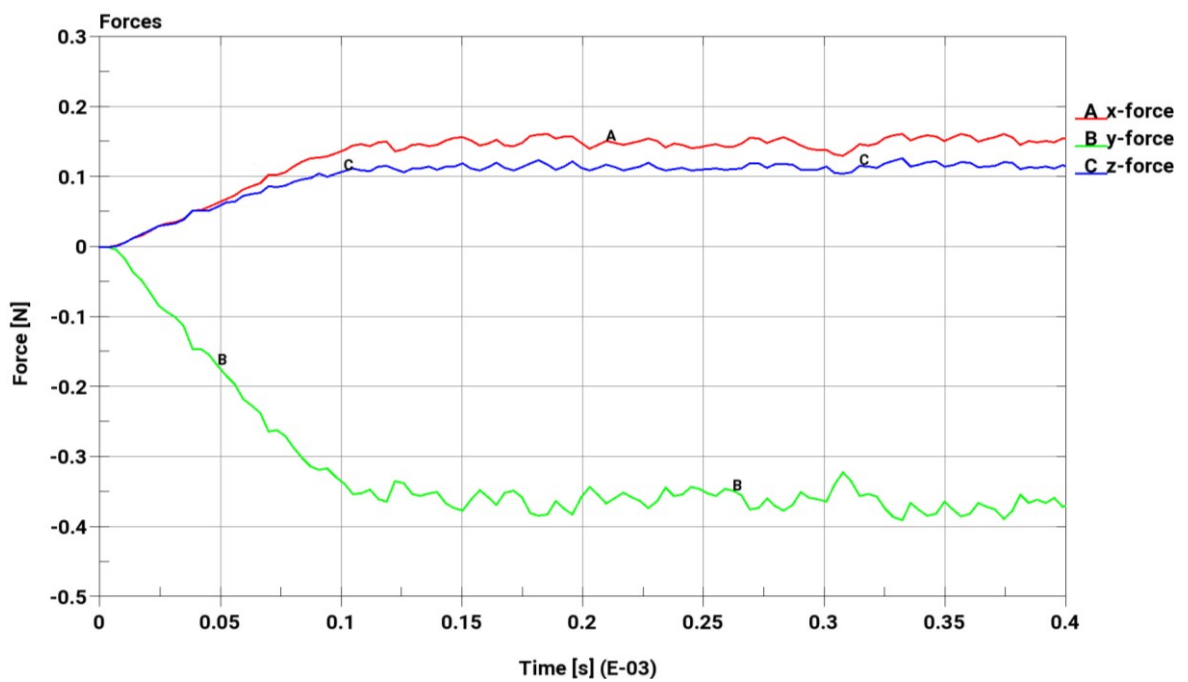
Standard setting for friction in our company is the value 0.2. This, however, is because mostly plastic parts are used in our company simulations. Friction coefficients between wood and steel range from 0.2 to 0.6. [19], [20] A more realistic friction coefficient 0.3 is chosen for version 2.01.

Results

The measured forces are compared with version 2.00 in Fig. 34.



a) Version 2.00



b) Version 2.01

Fig. 34 - Comparison of the forces from versions 2.00 and 2.01

The x-force and y-force decreased slightly and the z-force slightly increased. Version 2.01 is used as a new reference since the friction coefficient is considered more realistic. The final forces can be calibrated by changing the friction coefficient in the range from 0.2 to 0.6.

4.2.3 Version 2.02 – Thicker Wood

In the model, the nodes in the set defined for the movement of the wood have all movements in the x and y direction constrained. In order to find out whether the wood is thick enough to minimise the rigid response of the upper surface, a simulation with the thickness of the wood doubled is run.

Results

Almost no influence is observed on the cutting forces. It is therefore assumed that the original thickness is sufficient.

4.2.4 Timestep variation

Versions with the timestep $4.0 \cdot 10^{-8}$ s and $1.0 \cdot 10^{-8}$ s are run to see the influence of the timestep on the contact forces.

Results

With the timestep $4.0 \cdot 10^{-8}$ s the excessive element erosion reoccurred, and the contact forces decreased significantly. With the timestep $1.0 \cdot 10^{-8}$ s a slight increase was observed on all forces (approx. 10 %). The timestep will need to be decreased for calibrating the final forces. For investigating the influence of the parameters on the contact forces, the original timestep is considered sufficient.

4.2.5 Mesh size variation

Five versions with different mesh sizes were run to investigate, if and in which manner is the simulation mesh-size dependent. The mesh versions are:

- The x dimension doubled – 0.12x0.25x0.1 mm
- The x dimension halved – 0.03x0.25 x0.1 mm
- The y dimension halved – 0.06x0.125x0.1 mm
- The z dimension doubled – 0.06x0.25x0.2 mm
- The z dimension halved – 0.06x0.25x0.05 mm

In each direction, the dimension was doubled and halved, except for the y direction, in which the dimension would be 0.5 mm if doubled, which seemed too high for this kind of simulation in addition to a poor aspect ratio, that would arise.

When the x dimension is halved, the minimal element edge length decreases from 0.06 mm to 0.03 mm so the timestep must be decreased accordingly. The decrease to 0.05 mm when the z direction is halved is considered negligible.

Results

Surprisingly, the doubling and halving of the x dimension both caused an increase in all the cutting forces with the difference being more significant for the halving. An explanation could be that while the doubling causes a need for more volume of elements to erode, leading to less accuracy, the halving causes a poorer aspect ratio for the elements.

Halving the y direction leads to a considerable decrease in all the cutting forces (approx. 20-30 %).

In the z direction, when the direction is doubled, a significant increase occurs. When the direction is halved, however, no significant change is observed.

Generally, a refinement of the mesh leads to a reduction of the fluctuations and vice versa.

The wood is clearly mesh-size sensitive for this kind of simulation in both the x and y directions. In the z direction, the mesh is assumed to be fine enough. For more accurate results, a finer mesh would be needed, but a significant increase in computation time would follow. Since the calibrated material model is intended for large and complicated model, excessive increase in computation time would make the material model useless. Refinement of the model of the wood must be done cautiously.

4.2.6 Contact definition

Besides CONTACT_ERODING_NODES_TO_SURFACE, LS Dyna offers two more eroding contact definitions:

- CONTACT_ERODING_SINGLE_SURFACE
- CONTACT_ERODING_SURFACE_TO_SURFACE

Since no forces can be output for the single surface contact, because it has only one surface which generates both the action and reaction which nullify each other in the resultant forces, the only other option is the surface to surface contact. A contact of the surfaces is generally closer to reality since no parts can penetrate without a force being generated.

However, for the eroding elements, computation difficulties may occur as the normal of the surface changes its direction rapidly.

Results

Larger fluctuations occurred in the cutting forces and the x-force was decreased dramatically. The forces are shown in Fig. 35.

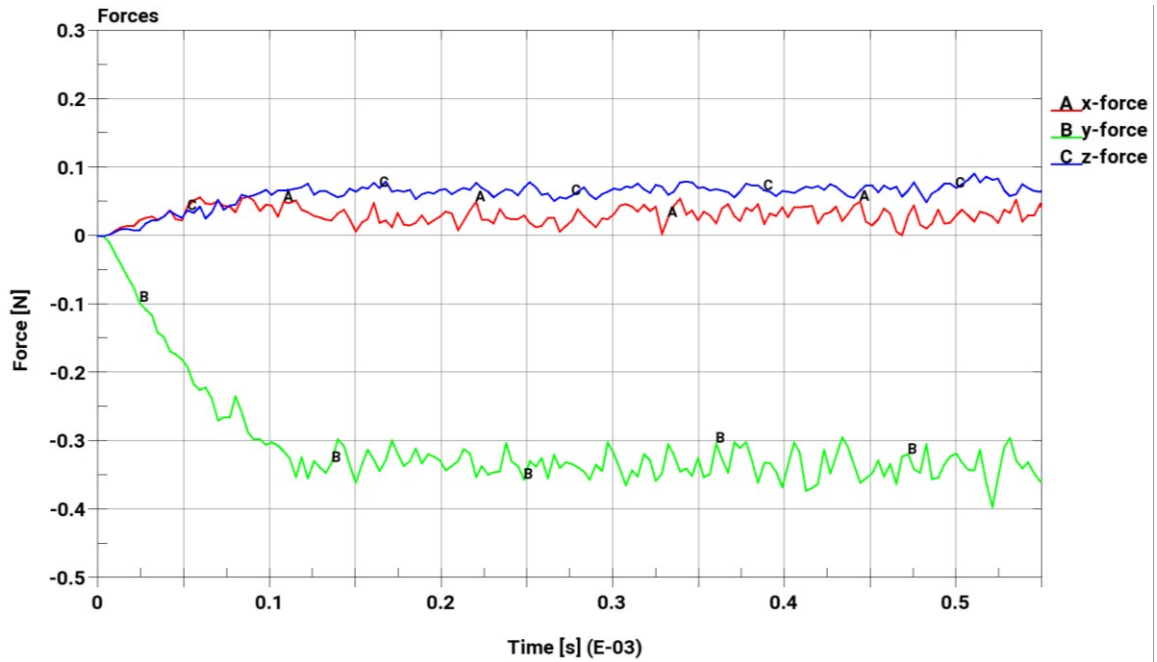


Fig. 35 - Surface to surface contact forces

According to the experiment, the x-force should be higher than the z-force. The nodes to surface contact is assumed to be a better fit for this simulation.

4.2.7 Contact scaling

In the contact keyword, there is an option to scale the contact stiffness. It seems logical that this could influence the contact forces. Scale factors 2 and 4 were used.

Results

The contact scaling had little to no effect on the resultant forces.

4.2.8 Elastic Moduli

The next step after investigating the influence of the simulation settings on the contact forces is to investigate the material model.

There are a lot of parameters that can be investigated. It would be beyond the scope of this thesis to investigate each parameter individually. Some parameters are therefore modified in groups. The first group of parameters is the elastic moduli. It is logical that the stiffness of a material could influence the cutting forces.

The normal moduli were discussed in chapters 4.1.4 and 4.1.7.

The values for the parallel shear modulus (G_{LT}) in the literature range from 642 to 1640 $\text{N} \cdot \text{mm}^{-2}$ with the G_{LT} and G_{LR} values being relatively close and no moisture dependency assumed. The optimal value is searched in this range.

The perpendicular shear modulus (G_{TR}) ranges from 234 to 620 $\text{N} \cdot \text{mm}^{-2}$.

Table 4 shows the elastic moduli used in the following versions.

Table 4 - The elastic moduli for versions 2.13 and 2.14

	E_L	E_T	G_{LT}	G_{TR}
Version 2.13	13,200	1,560	1200	600
Version 2.14	9,000	1,000	800	350

Results

The forces decrease with increasing stiffness and vice versa. In version 2.13 all forces decrease by approx. 10 to 20 %. In version 2.14 the forces increase by approx. 10 %.

4.2.9 Failure Criteria

The influence of the failure criteria should be predictable. An increase of the forces with increasing strength is expected.

The tensile strength is the only parameter exhibiting moisture dependency. The data consist of values from one source and one value from one another source for the longitudinal direction which decreased the CoD of the moisture dependency significantly. It must be taken into consideration that if data from other sources were available, the CoD of the moisture dependency could decrease further.

The ranges for the compressive and shear strengths are wide. The ranges are summarised in Table 5.

Table 5 - Ranges of the material strengths in $N \cdot mm^{-2}$; the value in the brackets is from one source [21] and differs considerably

X_T	X_C	Y_T	Y_C	S_{XY}	S_{YZ}
80 – 121	45 – 74	7.3 – 21.4	6 – 12.9 (52.4)	14.2 – 20.8	5.6 – 24

Suggestions from the LS Dyna manual are also taken into consideration.

One suggestion is that the Y_T value should be 30 to 50 times lower than X_T . This would mean that the Y_T value should not exceed $4 N \cdot mm^{-2}$. Values lower than $7.3 N \cdot mm^{-2}$ are plausible since the value decreases with increasing MC.

The manual also suggests that Y_C should be 4 to 5 times lower than X_C . Values close to $Y_C = 52.4 N \cdot mm^{-2}$ should be avoided.

The values used in version 2.15 are listed in Table 6.

Table 6 - Card 3 for version 2.15

X_T	X_C	Y_T	Y_C	S_{XY}	S_{YZ}
120	60	6	12	15	15

Results

The increase of the strength parameters led to an increase of the contact forces as expected. An increase by approx. 20 % led to a 20 to 30 % increase of the forces.

4.2.10 Poisson's Ratio

The Poisson's ratio is discussed in chapter 4.1.6. It could also influence the contact forces since it influences the deformation of the elements. Values 0.2 and 0.05 are used in the simulations.

Results

The change of the Poisson's ratio had no significant effect on the contact forces.

4.2.11 Softening Parameters

LS Dyna defines the fracture energy as the area under the stress-displacement curve as it softens from peak stress to zero stress. Values approximated from fracture intensities were found in [16].

Parameters B and D influence the shape of the stress-displacement curve. LS Dyna recommends the range from 10 to 50.

The postpeak damage parameters d_{MAX} the maximum damage that can accumulate. The recommended values $d_{MAX\parallel} = 0.9999$ and $d_{MAX\perp} = 0.99$ are used.

The softening parameters are discussed in more detail in [11].

Version 2.16 has the fracture energies from the material example. In version 2.17 the B and D parameters are increased to 50.

Results

In version 2.16, the significant decrease of fracture energies led to a decrease of the contact forces by approx. 30 to 40 %.

In version 2.17, no significant effect on the contact forces was observed.

4.2.12 Hardening Parameters

The prepeak hardening parameters N and c determinate the initiation and the rate of prepeak hardening. The way in which they influence the stress-strain curve is described in Fig. 36.

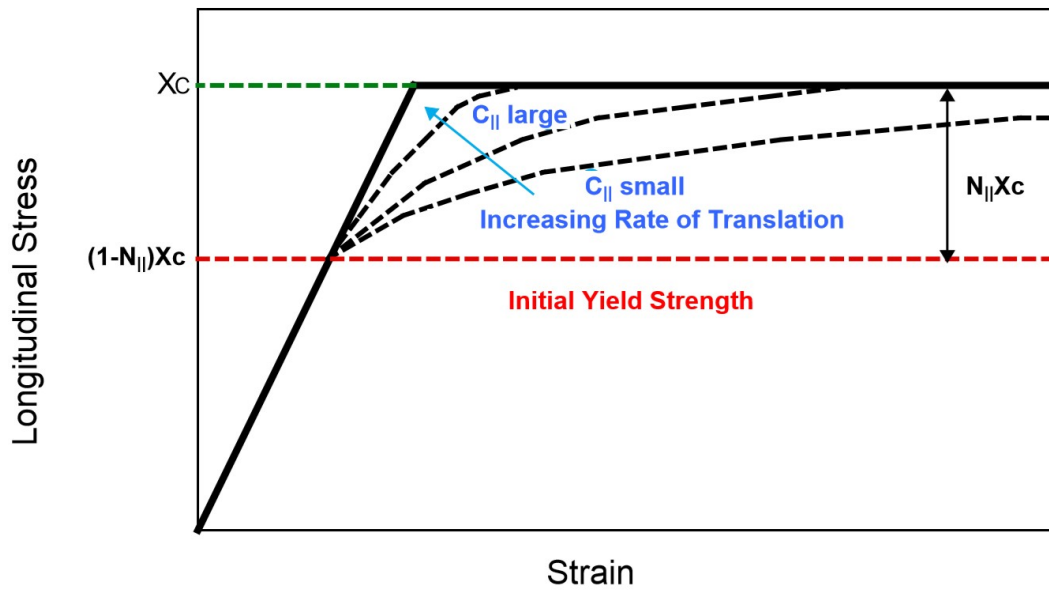


Fig. 36 - Influence of the prepeak hardening parameters on the stress-strain curve [11]

The manual suggests using the values 0.3 for both N values or the values can be taken from the example $N_{||} = 0.5$ and $N_{\perp} = 0.4$. For the c values, the recommended range is 100 to 1000.

GHARD is an additional hardening parameter that produces continued hardening that can surpass the ultimate yield surface. The manual recommends either a zero value for perfect plasticity in compression or a small positive value e.g. 0.02.

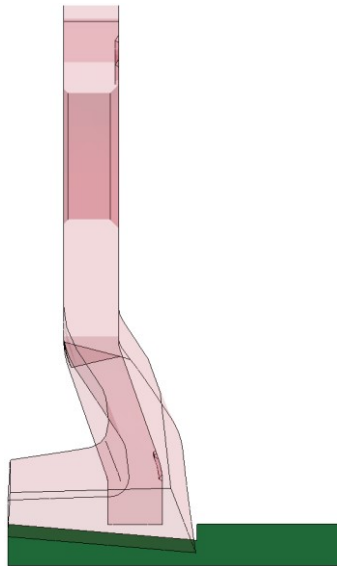
Version 2.18 has the hardening initiation parameters increased to $N_{||} = 0.5$ and $N_{\perp} = 0.4$. Versions 2.19 and 2.20 have the hardening rates set to 100 and 1000 respectively. In version 2.21 the GHARD parameter is set to 0.02.

Results

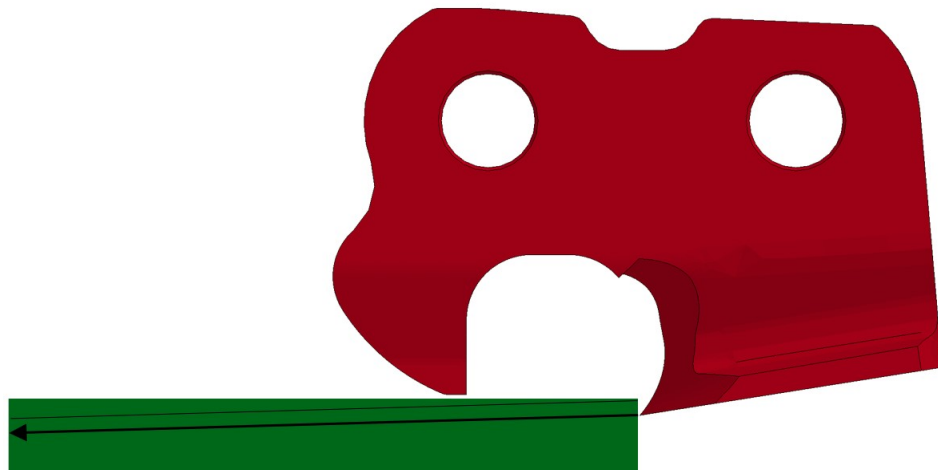
The earlier hardening initiation had no significant effect on the forces. Increasing the hardening rate led to a slight increase of the forces (approx. 10 % difference between versions 2.19 and 2.20). The GHARD parameter led to a decrease of the forces by approx. 20 %.

5 Final Version

Using the knowledge gained in chapter 4, the model is calibrated so that the numerically determined cutting forces match those that were measured experimentally as closely as possible.



a) Full engagement of the incisor



b) The edge of the precut parallel to an arrow showing the trajectory of the relative motion; the x direction is scaled for better clearness

Fig. 37 - Final model overview

5.1 Contact Forces

To compare the contact forces with the experimental data, the model must be modified to obtain a better match with the reality. The wood geometry is modified. The new geometry

is a representation of a precut wooden block so that the incisor is engaged evenly across the width and the cutting depth is 0.3 mm throughout the whole simulation. The model is shown in Fig. 37. The plane of the cut is parallel to the trajectory of the relative motion of the incisor and the wood.

5.1.1 Mesh

The wood geometry is a little more complicated and different meshes of the same size can be applied. Two versions of meshes that are as simple as possible are shown in Fig. 38.

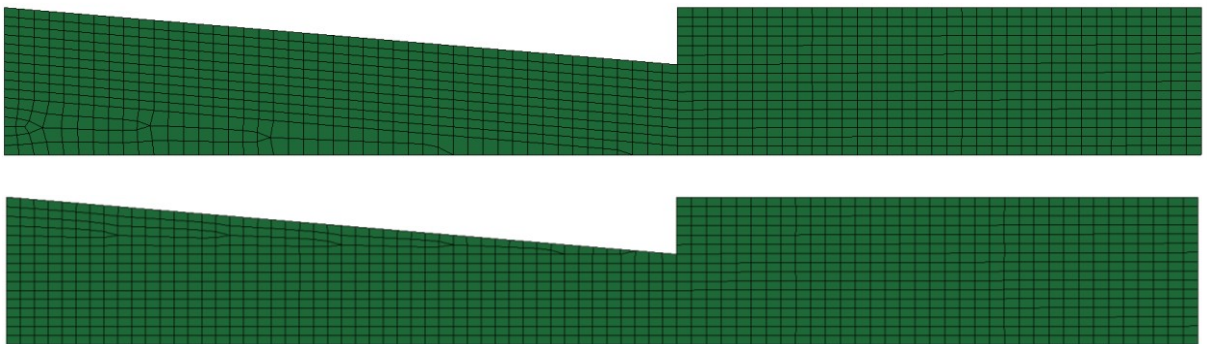


Fig. 38 - Comparison of the meshes for the final model

During the final calibration, it was discovered that with slightly different settings, a change from one mesh to the other can lead both to an increase or to a decrease of the contact forces.

The second version was chosen as it is closer to the mesh that would be used in the simulation, for which the material model is intended for.

The basic dimensions of the mesh are 0.06x0.125x0.1 mm.

5.1.2 Simulation Settings

The timestep is set to $3 \cdot 10^{-9}$ s. The friction is set to 0.4. The material data are shown in Fig. 39.

```

*MAT_WOOD
$-->--1-->--2-->--3-->--4-->--5-->--6-->--7-->--8
$  mid|    ro|    nplot|   iters|   irate|   ghard|   ifail|   ivol|
   99902  0.67E-09    1      1      0      0.02    1      1
$-->--1-->--2-->--3-->--4-->--5-->--6-->--7-->--8
$  el|    et|    glt|    gtr|    pr|
   9000   1560   1200    600    0.40
$-->--1-->--2-->--3-->--4-->--5-->--6-->--7-->--8
$  xt|    xc|    yt|    yc|    sxy|    syz|
   100    55     6     7     15    15
$-->--1-->--2-->--3-->--4-->--5-->--6-->--7-->--8
$  gf1|||  gf2|||  bfit|  dmax|||  gf1-||  gf2-||  dfit|  dmax-||
    50     90     30  0.9999  0.45    0.9     30    0.99
$-->--1-->--2-->--3-->--4-->--5-->--6-->--7-->--8
$  flpar|  flparc|  powpar|  flper|  flperc|  power|
$
$-->--1-->--2-->--3-->--4-->--5-->--6-->--7-->--8
$  npar|   cpar|   nper|   cper|
    0.3   400.0   0.3   100.0
$-->--1-->--2-->--3-->--4-->--5-->--6-->--7-->--8
$  aopt|   macf|   beta|
    2     1
$-->--1-->--2-->--3-->--4-->--5-->--6-->--7-->--8
$  xp|    yp|    zp|    a1|    a2|    a3|
         0     0     1
$-->--1-->--2-->--3-->--4-->--5-->--6-->--7-->--8
$  d1|    d2|    d3|    v1|    v2|    v3|
    0     1     0
$

```

Fig. 39 - Final version of the material

5.1.3 Evaluation

Mean values are calculated on the time interval where the force fluctuates around a constant value and are compared with the experiment.

5.1.4 Results

The contact forces are shown in Fig. 40.

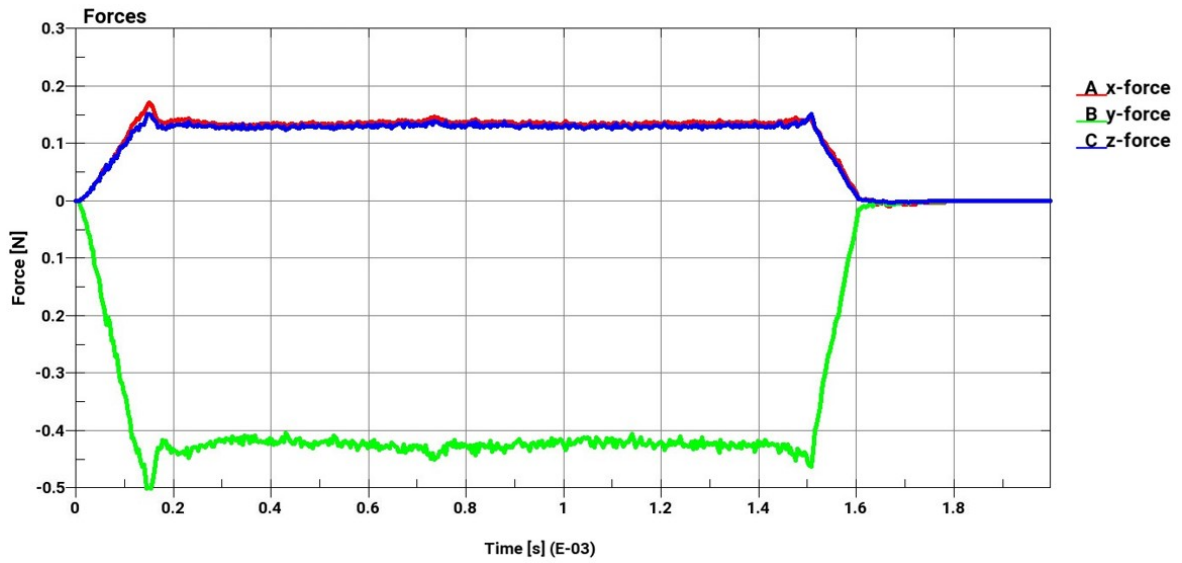


Fig. 40 - Contact forces

It can be seen that since the cutting depth is constant, the contact forces do not increase during the simulation, when the incisor is engaged.

Table 7 shows the comparison of the cutting forces with the experiment.

Table 7 - Comparison of the forces from the experiment and the simulation

	x-force [N]	y-force [N]	z-force [N]
Experiment	0.11 – 0.14	0.33 – 0.37	0.05 – 0.07
Simulation	0.14	0.42	0.13

The forces in the x and y directions show an exceptionally good match, being 1 % and 14 % above the maximal measured value. The z-force from the simulation is 92 % above the maximal measured value. The z-force showed a slight decrease with the decreasing diameter of the wood so the force might be slightly influenced by the simplification of the model with the translation instead of the rotation. Another factor influencing the force is the mesh dependency, with the forces varying not only with different mesh sizes, but also with different orientation (as was shown in chapter 5.1.1). Another factor could be using the transversely isotropic material model instead of an orthotropic one.

Ways of decreasing the z-force are known from chapter 4.2. However, it would also influence the other two forces. The incisors on a chainsaw are aligned in such a way, that every two consecutive incisors are symmetrical about the x-y plane (Fig. 41).



Fig. 41 - The configuration of the incisors on a saw chain [22]

This configuration is also used in the simulation, for which the material model is intended, and it ensures that the z-forces acting on the saw chain are nullified. Therefore, the difference of the z-forces is considered acceptable.

5.2 Chip Formation

For a comparison of the chip with the highspeed camera recordings, the model is slightly changed. The tool is added to the simulation as an elastic part. The feed velocity prescription is applied on a nodal set on the tool instead of the incisor. The movement of the incisor is not constrained in general directions. Instead, a set of nodes on the tool is added to the rigid incisor by the keyword `CONSTRAINED_EXTRA_NODES_SET` to represent a connection by bolts. A contact between the tool and the wood is also defined.

5.2.1 Results

A comparison of the chips is shown in Fig. 42.

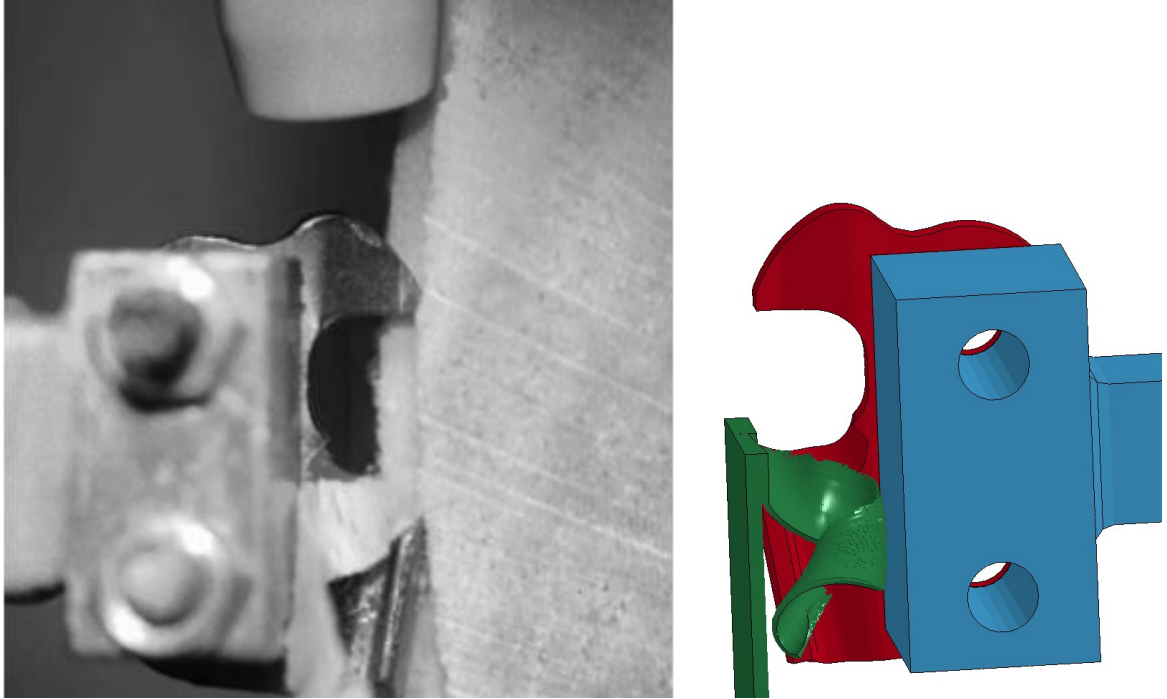


Fig. 42 - Comparison of the chips

The chip from the simulation matches the experiment relatively well. It can be seen that the chip from the simulation is slightly more curved. The reason could be that the chip is not in contact with the tool for a time long enough to stabilize. A simulation with a longer piece of wood does not need to be run since the match is already relatively good.

6 Conclusion

The aim of this thesis was to research the ranges of material properties of European beech wood. Properties of wood vary from piece to piece, so a range of values was found, rather than exact values.

Then the aim was to run numerical simulations of wood cutting, vary the material properties in the ranges found, as well as other simulation settings, and determine how those parameters influence the cutting forces.

The final goal was to apply the gained knowledge and calibrate a simulation of wood cutting to match the cutting forces and the chip formation with the experiment.

Material data was extracted from 19 different sources and analysed. The data was put together and a first material model was created.

Then, influence of 7 parameters on the chip formation and 11 parameters or groups of parameters on the cutting forces was investigated.

The gained knowledge was applied for calibration. The result was a model with a particularly good match in the x-force and y-force. The match in the z-force was sufficient for the oncoming simulations. The calibration of the chip formation was also successful.

An important discovery was that the simulation is mesh size and mesh orientation dependent for this material. A further investigation on this topic is required before the material model can be implemented to the experiment of chainsaw cutting.

References

- [1] HERING, S. *Charakterisierung und Modellierung der Materialeigenschaften von Rotbuchenholz zur Simulation von Holzverklebungen*. Dohna, Germany, 2011. Doctoral thesis. Technische Universität Dresden.
- [2] OZYHAR, T., S. HERING, S. SANABRIA a P. NIEMZ. Determining moisture-dependent elastic characteristics of beech wood by means of ultrasonic waves. *Wood Science and Technology*. 2013, **47**(2), 329-341.
- [3] Non-linear Mechanical Behaviour of Wood. *Non Linear Mechanical Behaviour of Wood* [online]. Vila Real: Universidade de Trás-os-Montes e Alto Douro, 2000 [cit. 2019-12-12]. Dostupné z: http://jmcx.utad.pt/nlmbwood/english/Project_e.htm
- [4] OZYHAR, T., S. HERING a P. NIEMZ. Moisture-dependent elastic and strength anisotropy of European beech wood in tension. *Journal of Materials Science*. 2012, **47**(16), 6141-6150. DOI: <https://doi.org/10.1007/s10853-012-6534-8>.
- [5] BRABEC, M., R. LAGAÑA, J. MILICH, J. TIPPNER a V. SEBERA. Utilization of digital image correlation in determining of both longitudinal shear moduli of wood at single torsion test. *Wood Science and Technology*. 2017, **51**(1), 29-45.
- [6] TANG, Z., J. LIANG, Z. XIAO a C. GUO. Large deformation measurement scheme for 3D digital image correlation method. *Optics and Lasers in Engineering*. 2012, **50**(2), 122-130.
- [7] NIEMZ, P., T. OZYHAR, S. HERING a W. SONDEREGGER. Zur Orthotropie der physikalisch-mechanischen Eigenschaften von Rotbuchenholz. *Bautechnik*. 2015, **92**(1), 3-8.
- [8] Wood Testing Accessories - Instron. *Instron: Materials Testing Machines for Tensile, Fatigue, Impact, ...* [online]. Norwood: Instron, 2019 [cit. 2019-12-12]. Dostupné z: <https://www.instron.co.hu/hu-hu/products/testing-accessories/application-specific-accessories/wood>
- [9] KOLLMAN, F., E. KUENZI a A. STAMM. *Principles of Wood Science and Technology: II Wood Based Materials*. 1st edition. Berlin/Heidelberg: Springer-Verlag, 1975. ISBN 978-3-642-87931-9.
- [10] KRÜGER, R., B. BUCHELT a A. WAGENFÜHR. New method for determination of shear properties of wood. *Wood Science and Technology*. 2018, **52**(6), 1555-1568.
- [11] *Manual for LS-DYNA: Wood Material Model 143*.
- [12] PADOVEC, Z. *Kompozitní materiály: Presentation presented at [Vybrané statě z pružnosti a pevnosti, 2019, Prague, Czech Republic]*.
- [13] *LS-DYNA: Theory Manual*.

- [14] *Nonlinear Implicit Analyses: LS-DYNA Training*. Stuttgart, 2017.
- [15] OLIVAN, M. *Systemanalyse einer Sägekette im Hinblick auf Modellierung eines FEM-Modells für Schneidezähne*. Weingarten-Ravensburg, 2015. Master Thesis. Hochschule Weingarten-Ravensburg.
- [16] HARTIG, J., S FACCHINI a P HALLER. Investigations on lateral vehicle impact on moulded wooden tubes made of beech (*Fagus sylvatica* L.). *Construction and Building Materials*. 2018, **174**, 547-558.
- [17] *LS-DYNA KEYWORD USER'S MANUAL*. VOLUME I.
- [18] PICHLER, P., M. LEITNER, F. GRÜN a C. GUSTER. Evaluation of wood material models for the numerical assessment of cutting forces in chipping processes. *Wood Science and Technology*. 2018, **52**(1), 281-294.
- [19] Friction and Friction Coefficients. *Engineering Toolbox* [online]. 2004 [cit. 2020-07-29]. Dostupné z: https://www.engineeringtoolbox.com/friction-coefficients-d_778.html
- [20] Coefficient for Static Friction of Steel Chart. *Carbide Depot Technical Resources for Manufacturing Professionals* [online]. [cit. 2020-07-29]. Dostupné z: <http://www.carbidedepot.com/formulas-frictioncoefficient.htm>
- [21] HOLAN, J. a L. MERENTA. Selected mechanical properties of modified beech wood. *Acta univ. agric. et silvic. Mendel. Brun.* 2008, **56**(1), 245-250.
- [22] Řetěz na motorovou pilu Stihl. *Zahradní technika STIHL Konice - vše pro les, zahradu a volný čas* [online]. Konice [cit. 2020-07-28]. Dostupné z: <https://www.e-les.cz/Retez-pilovy-Stihl-325-1-5mm-64cl-HRANATY-RS-36380000064-d1581.htm>
- [23] HÖRIG, H. Anwendung der Elastizitätstheorie anisotroper Körper auf Messungen an Holz. *Ingenieur-Archiv*. 1935, **6**(1), 8-14.
- [24] HEARMON, R. a W. BARKAS. The effect of grain direction on the Young's moduli and rigidity moduli of beech and sitka spruce. *Proceeding of the physical society*. 1941, **53**(6), 674.
- [25] NEUMANN, A. *Ermittlung und Bewertung der elastischen Materialkennwerte von Vollholz in Abhängigkeit der Feuchte und der Anisotropie (Identification and evaluation of the elastic properties of solid wood depending on the moisture and anisotropy)*. Dresden, 1998. Master Thesis. Technische Universität Dresden.
- [26] STAMER, J. a H. SIEGERSCHMIDT. Elastische Formänderung der Hölzer. *Ver. Dtsch Ing.* 1933, **77**, 503-505.
- [27] HUBER, K. Verdrehungselastizität und-festigkeit von Hölzern. *Wolf*. 1928.
- [28] BODIG, J. a J. GOODMAN. Prediction of elastic parameters for wood. *Wood Science*. 1973, **5**(4), 249-264.

- [29] HERING, S., D. KEUNECKE a P. NIEMZ. Moisture-dependent orthotropic elasticity of beech wood. *Wood Science and Technology*. 2012, **46**(5), 927-938.
- [30] BUCUR, V. a R. ARCHNER. Elastic constants for wood by an ultrasonic method. *Wood Science and Technology*. 1984, **18**(4), 255-265.
- [31] AICHNER, S., Z. CHRISTIAN a M. HIRSCH. Rolling shear modulus and strength of beech wood laminations. *Holzforschung*. 2016, **70**(8), 773-781.
- [32] POŽGAJ, A. *Štruktúra a vlastnosti dreva*. Bratislava: Príroda a.s., 1993.
- [33] HORVATH, N., S. MOLNÁR a P. NIEMZ. Untersuchungen zum Einfluss der Holzfeuchte auf ausgewählte Eigenschaften von Fichte Eiche und Rotbuche. *Holztechnologie*. 2008, **49**(1), 10-15.

List of Figures

Figure 1 – View of the experimental setup used to determine the cutting forces acting on a single chainsaw tooth	11
Figure 2 – The material axes of wood	12
Figure 3 – Moisture dependent density	13
Figure 4 – Moisture dependent normal elastic moduli	14
Figure 5 – Moisture dependent elastic shear moduli	15
Figure 6 – Moisture dependent Poisson's ratios	16
Figure 7 – Moisture dependent tensile strengths	17
Figure 8 – Moisture dependent shear strengths	17
Figure 9 – The principle of digital image correlation	18
Figure 10 – The specimen used for tensile test	19
Figure 11 – The compressive test setup – an illustrative image	19
Figure 12 – Stress-strain curves at different MC of European beech wood in compression in radial (left) and tangential (right) direction	20
Figure 13 – The Torsion test setup	21
Figure 14 – The test setup an (left), the sample (middle), and the deformation of the measuring field (right)	22
Figure 15 – Comparison of an orthotropic (left) and a transversely isotropic (right) model of wood	24
Figure 16 – The incisor	30
Figure 17 – The experimental setup	31
Figure 18 – The measuring systems	32
Figure 19 – A sample photo from the highspeed camera recording	32
Figure 20 – Coordinate system of the incisor	34
Figure 21 – - Forces from the strain gauges (green) and the load cell (blue)	36
Figure 22 – Meshes of the incisor and the wood	39

Figure 23 – Version 1.XX model overview	40
Figure 24 – Material cards of MAT_WOOD	41
Figure 25 – The slightly modified example material model	43
Figure 26 – Unphysically stretched elements	45
Figure 27 – Material card with parameters for beech wood – version 1.02	46
Figure 28 – The strangely behaving chip	47
Figure 29 – The chips with different Poisson's ratios	49
Figure 30 – Comparison of the chips from versions 1.01 and 1.04	51
Figure 31 – Comparison of the chip with erosion caused by perpendicular damage allowed	51
Figure 32 – Comparison of the chips with different timesteps	52
Figure 33 – Contact forces in version 2.00	56
Figure 34 – Comparison of the forces from versions 2.00 (left) and 2.01 (right)	57
Figure 35 – Surface to surface contact forces	60
Figure 36 – Influence of the prepeak hardening parameters on the stress-strain curve	64
Figure 37 – Final model overview	65
Figure 38 – Comparison of the meshes for the final model	66
Figure 39 – Final version of the material	67
Figure 40 – Contact forces	68
Figure 41 – The configuration of the incisors on a saw chain	69
Figure 42 – Comparison of the chips	70

List of Tables

Table 1 – The maximal and minimal forces in each direction (normalized)	36
Table 2 – Influence of individual parameters or set of parameters on the cutting forces	53
Table 3 – Influence of individual parameters or set of parameters on the cutting forces – cont.	54
Table 4 – The elastic moduli for versions 2.13 and 2.14	61
Table 5 – Ranges of the material strengths in $\text{N} \cdot \text{mm}^{-2}$; the value in the brackets is from one source and differs considerably	62
Table 6 – Card 3 for version 2.15	62
Table 7 – Comparison of the forces from the experiment and the simulation	68

Appendix I – Tables of the mechanical properties of the beech wood

The Elastic Moduli

<i>MC</i> [%]	<i>E_L</i> [MPa]	<i>E_T</i> [MPa]	<i>E_R</i> [MPa]	<i>G_{LT}</i> [MPa]	<i>G_{LR}</i> [MPa]	<i>G_{TR}</i> [MPa]	References
10.5				642	722		[23]
12				757	977		[5]
12	11 900	1030	1700	760	980	370	[24]
12				770	1110		[25]
12				700	1250		[26]
11				1080	1640		[27]
12				720	750		[25]
12				754	1013		[28]
10.5				1056	1608		[23]
10.5				1059			[26]
12				855	1280		[29]
12				920	1320		[30]
5.9	12 020	810	1800				[4]
11.3	10 560	730	1510				[4]
14.3	9270	600	1340				[4]
16.3	9200	530	1240				[4]

MC [%]	E_L [MPa]	E_T [MPa]	E_R [MPa]	G_{LT} [MPa]	G_{LR} [MPa]	G_{TR} [MPa]	References
9.6	11 180	560	2310	1010	1370	430	[2]
12.7	9560	490	2200	930	1240	380	[2]
16.8	8200	440	2040	90	1110	350	[2]
18.7	8800	420	1890	850	980	330	[2]
10,5	13 700	1140	2240	700	1250	620	[26]
8.9				664			[10]
8.6				688	953		[10]
8.9				658		234	[10]
9.75						339.5	[31]
12				762	975	366	[24]
11.9				860	1280	490	[29]

The Poisson's Ratios

MC [%]	ν_{LT} [-]	ν_{LR} [-]	ν_{TL} [-]	ν_{TR} [-]	ν_{RL} [-]	ν_{RT} [-]	References
9.6	0.11	0.01	2.21	1.09	0.04	0.26	[2]
12.7	0.11	0.02	2.26	1.02	0.08	0.23	[2]
16.8	0.13	0.03	2.43	0.90	0.11	0.20	[2]
18.7	0.12	0.04	2.37	0.77	0.20	0.17	[2]
5.9	0.04	0.04	0.59	0.53	0.43	0.24	[4]
11.3	0.04	0.04	0.58	0.61	0.43	0.31	[4]
14.3	0.04	0.05	0.62	0.65	0.39	0.36	[4]
16.3	0.05	0.04	0.87	0.70	0.47	0.36	[4]
10.5	0.04	0.07	0.51	0.75	0.45	0.36	[26]

Tensile Strength

<i>MC</i> [%]	σ_{LUTS} [MPa]	σ_{TUTS} [MPa]	σ_{RUTS} [MPa]	References
6.5	105			[18]
5.9	115.3	11.4	21.4	[4]
11.3	96.7	8.9	19.5	[4]
14.3	83.6	7.8	17.1	[4]
16.3	80.6	7.3	15.6	[4]
12	121			[21]

Compressive Strength

<i>MC</i> [%]	σ_{LUCS} [MPa]	σ_{TUCS} [MPa]	σ_{RUCS} [MPa]	References
12	74	52.3	52.4	[21]
11.3	45	6	11	[2]
12	56.7	12.9	8.5	[32]

Shear Strength

MC [%]	τ_{TR} [MPa]	τ_{LR} [MPa]	τ_{LT} [MPa]	References
12	22			[21]
12	23			[5]
11	24			[5]
12	8			[5]
12	8			[9]
12	9			[5]
12	12			[5]
12	13			[5]
12	13			[5]
12	14			[5]
12	14			[5]
8.9			16.6	[10]
8.6		20.8	17.1	[10]
8.9	6.6		16.6	[10]
11.2	7.1	19.7	14.81	[33]
13.9	5.6	15.7	14.2	[1]
9.75	5.7			[31]